Article

Non-leaching, Highly Biocompatible Nanocellulose Surfaces That Efficiently Resist Fouling by Bacteria in an Artificial Dermis Model

Ghada Hassan, Nina Forsman, Xing Wan, Leena Keurulainen, Luis M. Bimbo, Susanne Stehl, Frits van Charante, Michael Chrubasik, Aruna S. Prakash, Leena-Sisko Johansson, Declan C. Mullen, Blair F. Johnston, Ralf Zimmermann, Carsten Werner, Jari Yli-Kauhaluoma, Tom Coenye, Per E. J. Saris, Monika Österberg,* and Vânia M. Moreira*

ACCESS | Metrics & More | Article Recommendations | Supporting Information

ABSTRACT: Bacterial biofilm infections incur massive costs on healthcare systems worldwide. Particularly worrisome are the infections associated with pressure ulcers and prosthetic, plastic, and reconstructive surgeries, where staphylococci are the major biofilm-forming pathogens. Non-leaching antimicrobial surfaces offer great promise for the design of bioactive coatings to be used in medical devices. However, the vast majority are cationic, which brings about undesirable toxicity. To circumvent this issue, we have developed antimicrobial nanocellulose films by direct functionalization of the surface with dehydroabietic acid derivatives. Our conceptually unique design generates non-leaching anionic surfaces that reduce the number of viable staphylococci in suspension, including drug-resistant *Staphylococcus aureus*, by an impressive 4−5 log units, upon contact. Moreover, the films clearly prevent bacterial colonization of the surface in a model mimicking the physiological environment in chronic wounds. Their activity is not hampered by high protein content, and they nurture fibroblast growth at the surface without causing significant hemolysis. In this work, we have generated nanocellulose films with indisputable antimicrobial activity demonstrated using state-of-the-art models that best depict an "*in vivo* scenario". Our approach is to use fully renewable polymers and find suitable alternatives to silver and cationic antimicrobials.

Nanocellulose films + Dehydroabietic acid derivatives =
No bacterial colonization
4-5 log reduction in viable *S. aureus* and MRSA
Artificial dermis model

KEYWORDS: cellulose nanofibril, antimicrobial, surface, biofilm, dehydroabietic acid
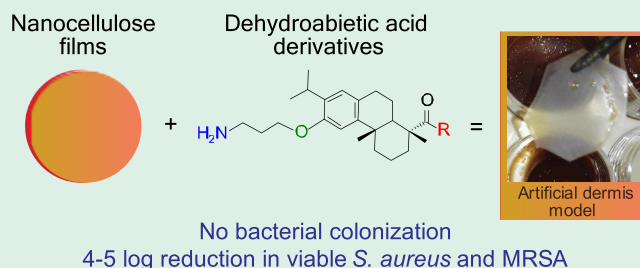
INTRODUCTION

Bacterial attachment and subsequent biofilm formation significantly hinder surface performance in a plethora of circumstances including food packaging, sanitary and household materials, as well as military and medical items.[1−4] As a consequence, the colonization of surfaces by bacteria has been under intensive research aiming at finding guiding principles to efficiently manipulate bacteria−surface interactions for the benefit of humans.[5−9] From a health perspective, the most worrisome biofilm-based infections are those associated with implanted medical devices; chronic wounds (including pressure ulcers); and prosthetic, plastic, and reconstructive surgeries.[10−13] Biofilms are difficult to treat once established as microorganisms in biofilms are inherently tolerant and resistant to antimicrobial therapies. In addition, dispersal of bacterial cells from biofilms carries a very significant risk of infection dissemination within the host. Not surprisingly, biofilm-based infections and associated complications currently incur massive financial costs on healthcare systems.[1−4] Therefore, clinical and economic benefits will surely accrue from improved anti-

microbial coatings that efficiently limit bacterial attachment as an alternative to treating mature biofilms.

The design of antimicrobial surfaces comprises chemical engineering of the surface to either leach biocides or kill bacteria directly upon contact.[3,4] Remarkable progress in this field has led to antibacterial surfaces with varying degrees of complexity[14−20] based, for instance, on enzymes, antimicrobial peptides, bacteriophages, polycations, graphene oxides, plasma technology, and several metal antimicrobials of which silver, despite its well-known toxicity to human cells and to the environment, is the most widely used. One of the major disadvantages of the leaching approach is that the surface progressively becomes ineffective as the antimicrobial species leaves the material, thereby severely limiting the surface
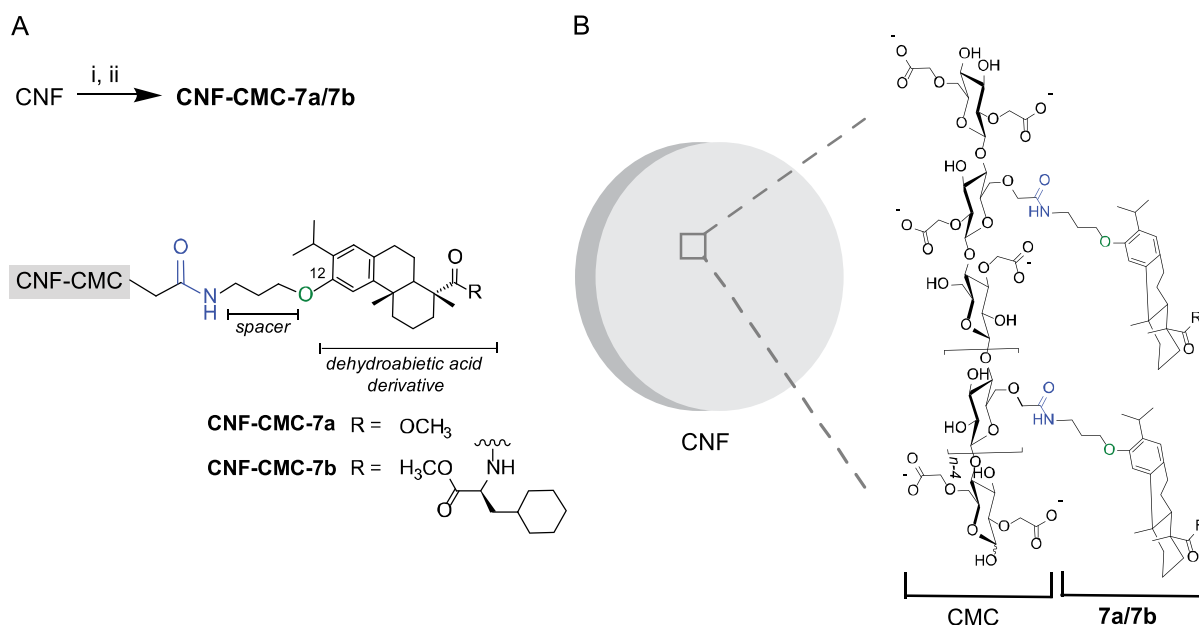
Figure 1. Synthesis of **CNF-CMC-7a** and **CNF-CMC-7b** and chemical detail of the surface composition. Reagents and conditions: (i) CaCl$_2$/NaHCO$_3$, Na-CMC, 80 °C, 4 h and (ii) EDC·HCl, DIPEA, HOBt, **7a** or **7b**, r.t., 24 h.

durability. In contrast, non-leaching contact-active surfaces are envisioned to be longer-lasting and even susceptible to reactivation by treatment with appropriate solvents, while protecting the environment from contamination with antimicrobials.

The tight electrostatic interactions that positively charged nanomaterials establish upon contact with the negatively charged functional groups at the surface of bacteria have been extensively exploited in the design of contact-active antibacterial surfaces, albeit the well-documented toxicity of polycationic compounds.[21−24] In contrast, anionic surfaces circumvent this toxicity issue because they fail to induce the strong membrane polarization that leads to cell lysis. Nonetheless, they remain greatly unexplored. A few reports document that nanoparticles with a negatively charged surface interact extensively through hydrogen bonding with lipopolysaccharides and/or peptidoglycans at the surface of bacteria that are responsible for structural integrity and survival, thus causing cell death, while bypassing general toxicity.[25,26] Carboxylate-functionalized polystyrene nanoparticles with a precise diameter have also been reported to interfere with specific surface proteins of fungi that influence key events in adhesion to abiotic surfaces and host tissues.[27]

In an era of increasing awareness of the need to replace petroleum-based polymers for alternatives widely abundant from natural sources, cellulose nanofibrils (CNFs), a fully renewable and biocompatible material, are an attractive starting point for the design of bioactive coatings.[28−32] Films made from CNFs combine sustainability with outstanding mechanical properties[33] and are envisioned to be able to replace synthetic polymer-based films in flexible electronics, medical devices, or food packaging.[28−32] Despite the fact that there are several reports detailing both leaching and non-leaching methods to make CNF antimicrobial,[34−40] CNF films that combine non-leaching and antimicrobial properties with good biocompatibility, in a way to preserve the physico-chemical properties needed for the envisioned applications, are currently lacking. In fact, only a few reports[37−39] detail the synthesis of

non-leaching antimicrobial CNF; however, these comprise highly cationic compounds[37] well known for their cyto- and ecotoxicities or are likely to have limited chemical stability because of the use of antimicrobial proteins[38] and grafting strategies based on reversible chemical reactions.[39] In this work, we present the first example of anionic CNF films modified with dehydroabietic acid derivatives that efficiently resist fouling by bacteria in an artificial dermis model mimicking the wound environment. We determine details of the chemical composition of the surface and discuss how these relate to the efficient antimicrobial activity observed. Recently, a wound dressing based on wood-derived CNF (FibDex)[41] was launched in the European market, showing the potential of CNF for the design of medical devices for human use alongside with bacterial cellulose and carboxymethyl cellulose (CMC).

RESULTS AND DISCUSSION

For the synthesis of **CNF-CMC-7a** and **CNF-CMC-7b** (Figure 1), an attachment point at C12 of the dehydroabietic acid derivative was designed, with a spacer length of three carbon atoms. In order to achieve this, dehydroabietic acid **1** was selected as the starting material for the synthesis of compounds **7a** and **7b**, by means of a six-step sequence (Figure 2).

Compound **7a** is capped with a methyl ester at C18, whereas compound **7b** bears a cyclohexyl-L-alanine moiety, previously reported to be relevant for the antimicrobial activity of dehydroabietanes.[42−45] For the synthesis of **7a**, compound **1** was first converted into its methyl ester **2a** to undergo Friedel−Crafts acylation reaction and give **3a**. Compound **2b** was prepared by N-(3-dimethylaminopropyl)-N′-ethylcarbodiimide (EDC)-mediated coupling of β-cyclohexyl-L-alanine methyl ester hydrochloride to **1**. Peracetic acid-mediated oxidation of **3a**/**3b** in acetic acid, followed by treatment with a base, gave **5a**/**5b**, which was reacted with t-Bu-(3-bromopropyl)-carbamate to give **6a**/**6b**. Compounds **7a**/**7b** were prepared after deprotection of the amino group by treatment with trifluoroacetic acid (TFA). Each compound was reacted with CNF films using carbodiimide chemistry after the surface was
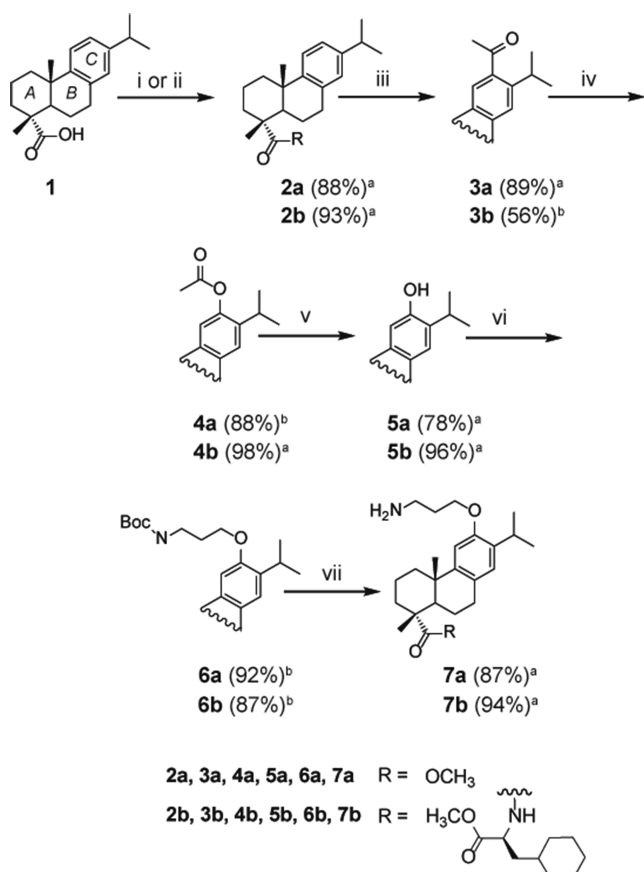
Figure 2. Synthesis of compounds **7a** and **7b**. Reagents and conditions: (i) CH$_3$I, K$_2$CO$_3$, DMF, r.t. for **2a**; (ii) EDC·HCl, DIPEA, HOBt, β-cyclohexyl-L-alanine methyl ester hydrochloride, DMF, r.t., 24 h for **2b**; (iii) AcCl, CH$_2$Cl$_2$, 0 °C to r.t.; (iv) AcOOH/AcOH, CH$_2$Cl$_2$, r.t; (v) K$_2$CO$_3$, MeOH, r.t.; (vi) t-Bu-(3-bromopropyl)carbamate, Cs$_2$CO$_3$, DMF, r.t; and (vii) TFA, CH$_2$Cl$_2$, 0 °C. [a]Crude yield. [b]Yield after chromatographic purification.

enriched in free carboxyl groups by adsorption of CMC (Figure 1).

X-ray photoelectron spectroscopy (XPS) was used to probe the surface composition prior to and after functionalization with compounds **7a** and **7b** (Table 1, Figure 3A,B). Specifically, nitrogen content and the presence of the ester groups were analyzed. Indeed, as expected, nitrogen was found on the functionalized films **CNF-CMC-7a** and **CNF-CMC-7b** only, and the content of C−C, that is, carbon atoms without oxygen neighbours, increased after the functionalization because of the presence of the dehydroabietic acid derivative bound at the surface. In good agreement, the content of carbon atoms with one bond to oxygen (C−O) was lower after the functionalization, while the content of carbon atoms with one

single and one double bond to oxygen (O−C═O), derived from carboxyl groups, increased. Using relative C−C or N content, it was estimated that **7a** covers no more than 20−30% of the surface of **CNF-CMC-7a**, whereas **7b** covers about 14−25% of the of the surface of **CNF-CMC-7b**.

Additional confirmation of the success of the coupling reaction was gathered from the time-of-flight secondary ion mass spectrometry (ToF-SIMS) analysis of CNF, **CNF-CMC**, **CNF-CMC-7b**, and single compound **7b** (Figure 3C,D and Figures S17, S18). A number of ions[46,47] were observed in the spectra of compound **7b**, including a peak corresponding to the protonated molecular ion [M + H]$^+$ at m/z 541.5 in the positive ion mass spectrum (Figure 3C). The corresponding deprotonated molecular ion peak [M − H]$^−$ was weakly observed in the negative ion spectrum at m/z 539.4 (Figure 3D). As expected, these peaks did not show up in either CNF or **CNF-CMC** but were present in the spectra of **CNF-CMC-7b**. Further evidence of the attachment of **7b** to the surface CMC was suggested by the peak at m/z 696.7 (Figure 3C), which was proposed to correspond to a monomeric CMC fragment bound to **7b** with a cleavage at its ring A amide bond, resulting in loss of the cyclohexylalanine group.

Electrokinetic (streaming current) measurements at varying pH values of 1 mM KCl solutions revealed a negatively charged interface for **CNF-CMC-7b** that can be attributed to the ionization of carboxyl groups (Figure 4A).[48,49] The interface generated by both **CNF-CMC** and **CNF-CMC-7b** showed a rather similar "electrokinetic fingerprint". The slight differences can be assigned to differences in the density and ionization of carboxyl groups as well as the impact of the interfacial structure on the electrohydrodynamics in the electrokinetic active region of the interface.[49] The lack of significant differences between both films corroborates the evidence collected from the XPS analysis, where it was estimated that the amount of compound **7b** that covers the surface is indeed relatively low.

As the functionalization of the films occurred only at the surface, no significant changes in the FTIR spectra were seen when comparing CNF, **CNF-CMC**, **CNF-CMC-7a**, and **CNF-CMC-7b** (Figure 4B). Surface morphology also remained unchanged (Figure S19). Nonetheless, as expected, the hydrophobicity of both **CNF-CMC-7a** and **CNF-CMC-7b** clearly increased in relation to CNF, as shown by the water contact angle values changing from 31.4 to 86.1 and 75.3°, respectively, due to the increased content of carbon and hydrogen at the surface of the abietane-containing films (Figure 4C). However, the static water contact angle measurements at 5 and 30 s showed that both **CNF-CMC-7a** and **CNF-CMC-7b** were still intrinsically hydrophilic (θ < 90°).[50]

The activity of **CNF-CMC-7b** was evident against planktonic Gram-positive staphylococci when compared to

Table 1. High Resolution Numerical XPS Data for CNF, CNF-CMC-7a, and CNF-CMC-7b

sample	wide scan atomic concentrations [%] (SD)[c]				high resolution C 1s carbon fits [%] (SD)[c]			
	C 1s	O 1s	N 1s	Si 2p	C−C	C−O	O−C−O	O−C═O
CNF	60.7 (0.5)	39.3 (0.5)	0.0 (0.0)	0 (0.0)	4.4 (0.0)	74.5 (0.2)	19.2 (0.1)	1.9 (0.0)
CNF-CMC-7a[a]	63.6 (1.3)	35.5 (1.3)	1.0 (0.0)	0 (0.0)	16.7 (1.1)	63.3 (1.1)	17.4 (0.1)	2.6 (0.1)
CNF-CMC-7b[b]	62.8 (0.4)	35.3 (0.3)	1.2 (0.1)	0.5 (0.2)	13.0 (0.6)	66.2 (1.0)	17.9 (0.7)	2.7 (0.2)

[a]Surface coverage for **CNF-CMC-7a** was estimated as 30% based on N content and 20% based on C−C content. [b]Surface coverage for **CNF-CMC-7b** was estimated as 25% based on N content and 14% based on C−C content. [c]Standard deviation (n = 3).
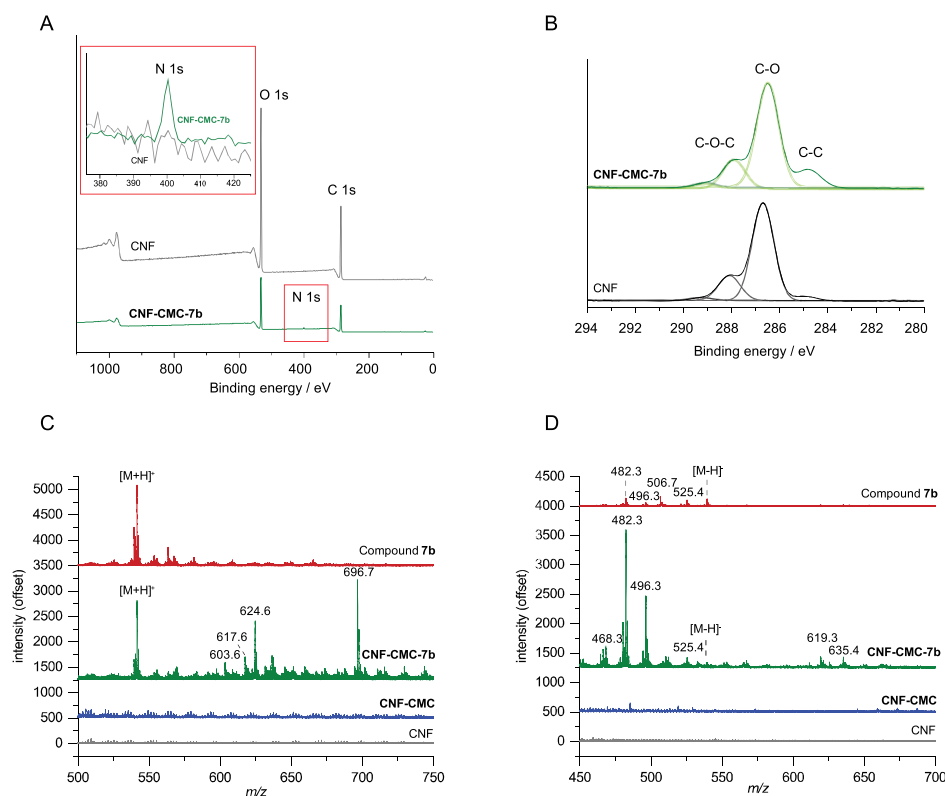
Figure 3. (A) XPS wide scan of CNF and **CNF-CMC-7b** with close-up of the N 1s signal. (B) High resolution C 1s spectra of CNF and **CNF-CMC-7b**. (C) Positive ion ToF-SIMS mass spectrum and (D) negative ion ToF-SIMS mass spectrum of CNF, **CNF-CMC**, **CNF-CMC-7b**, and compound **7b**.

unmodified CNF. **CNF-CMC-7b** films were able to produce approximately 4 and 5 log reductions in viable *Staphylococcus aureus* ATCC12598 cell counts and the methicillin-resistant strain MRSA 14TK301 strains after 24 h of contact, respectively (Figure 5A,B). Good activity was also observed against Gram-negative *Escherichia coli* with a reduction in bacterial counts of approximately 2 log units. **CNF-CMC-7a** was overall less potent but still able to target both Gram-positive and -negative bacteria. **CNF-CMC-7b** was selected for further studies including assessment of cell proliferation at the surface and toxicity toward blood cells (Figure 5C) as well as the ability to resist to bacterial colonization in both a biofilm model and an artificial dermis model that simulates a chronic wound environment[51] (Figure 6). Human fibroblasts prolif-erated to a larger extent at the surface of **CNF-CMC-7b** than they did at the surface of CNF, and only very minor haemolysis (1.8%) was induced by the presence of the modified films (Figure 5C).

In addition, the ability of **CNF-CMC-7b** to resist fouling by the virulent oxacillin-susceptible clinical isolate UAMS-1 was noteworthy. **CNF-CMC-7b** caused an average reduction in recovered CFU of 2.5 log units when compared to CNF in the biofilm model (Figure 6A). This result translated well into the wound model where **CNF-CMC-7b** was placed on top of the artificial dermis, and there was a clear reduction in the CFU recovered (1.4 log units) when compared to CNF (Figure 6B). As evidenced in the pictures, **CNF-CMC-7b** efficiently resisted colonization by UAMS-1. It should be noted that the artificial dermis model uses high concentrations of plasma and horse blood to moisten the dermis, so evidently the activity of **CNF-CMC-7b** is not hampered by plasma protein binding. As expected, as **CNF-CMC-7b** contacted only with the outer

surface of the artificial dermis which is roughly 1 cm thick, there was no significant difference in CFU recovery between the artificial dermises contacted with either **CNF-CMC-7b** or CNF after 24 h of biofilm formation because of the non-leaching, contact-active properties of **CNF-CMC-7b** (Figure 6C).

The mode of antimicrobial action of the CNF films designed from compounds **7a** and **7b** does not necessarily have to recapitulate the mode of action of the isolated compounds as these do not leave the surface of the films and are therefore unlikely to permeate the bacterial wall. Indeed, compound **7a** is devoid of significant antimicrobial activity, whereas **7b** is active against Gram-positive strains only, including *S. aureus* ATCC12598, UAMS-1, and the methicillin-resistant, vanco-mycin (Van)-intermediate resistant *S. aureus* Mu50 (Table 2, Figure 7). Treatment of *S. aureus* ATCC12598 with a 7× minimum inhibitory concentrations (MIC) concentration of **7b** for a short period of time does not seem to cause extensive bacterial cell lysis, suggesting that it is a slow acting compound (Figure 7A). In sharp contrast, both **CNF-CMC-7a** and **CNF-CMC-7b** are active against Gram-positive and -negative bacteria. **CNF-CMC-7b** in particular is active against Gram-negative *E. coli* DH5α (Figure 5B), whereas compound **7b** is inactive even at a high concentration of 400 μM (Table 2).

Scanning electron micrographs of *S. aureus* ATCC12598 after exposure to **CNF-CMC-7b** showed extensive background debris and bacteria with rough surfaces and bubble-like protrusions, indicating severe damage to the cell wall (Figure 8). After treatment with **7b**, a few intact bacteria could be observed along with cell debris.

The key to understanding the potential mode of action of surfaces generated from CNF films and dehydroabietic acid
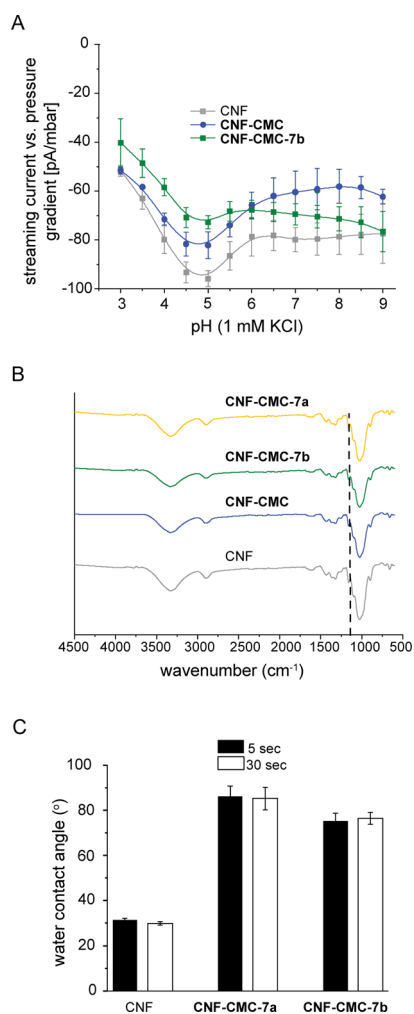
Figure 4. (A) Streaming current vs pressure gradient measurements for CNF, **CNF-CMC,** and **CNF-CMC-7b**; (B) Fourier-transform infrared (FTIR) spectra of CNF, **CNF-CMC**, **CNF-CMC-7a,** and **CNF-CMC-7b** with graphics normalized by the 1159 cm^{-1} band; (C) water contact angle measurements at 5 and 30 s for CNF, **CNF-CMC-7a,** and **CNF-CMC-7b**. **CNF-CMC** is very hydrophilic and does not allow accurate water contact angle determination.

Figure 5. (A) Amount of viable MRSA 14TK301 from 10% of ~10^5 colony forming units (CFU)/mL cell suspensions, after 24 h of incubation with CNF or **CNF-CMC-7b**. **CNF-CMC** was devoid of significant antimicrobial activity as previously reported;[57] (B) antimicrobial activity of CNF, **CNF-CMC-7a,** and **CNF-CMC-7b**. ◆; = not tested. Statistical analysis was made using a 2-tailed independent *t*-test where, **CNF-CMC-7a** and **CNF-CMC-7b** were compared to CNF, *p < 0.05. (C) Human fibroblast viability (measured in terms of percent of viable fibroblasts placed on top of each material compared to the percent of viable fibroblasts grown on a sterile tissue culture-treated 24-well control plate) and haemolysis testing (measured in terms of percent of haemolyzed erythrocytes from the 2% Triton X-100 solution) for CNF and **CNF-CMC-7b**. Statistical analysis was made by one-way ANOVA, followed by a Dunnett's multiple comparison test. All data sets were compared with CNF, and the levels of significance were set at probabilities of *p < 0.05, **p < 0.01, and ***p < 0.001, (n = 4), n.s.= not significant.

derivatives such as compounds **7a** or **7b** resides in close inspection of the details of the chemistry generated at the surface (Figure 1). This highly heterogeneous film surface comprises unreacted carboxyl groups from the adsorbed CMC (pK_a 3.6)[52] that will be ionized at pH 7 and a small number of nonionizable, amide-bonded **7a/7b** fingers, unevenly distributed throughout the CMC backbone. The overall surface is likely to be perceived by bacteria as a complex anionic sugar-based polymeric matrix unevenly branched with the compound, where hydrophilic and hydrophobic regions are not clearly separated but instead have a mosaic distribution of polarity, that is, **CNF-CMC-7a** and **CNF-CMC-7b** bear "imperfect amphipathicity".[53] This property has been described in biosurfactants produced by microorganisms, such as glycolipids, lipopeptides or saponins, and is responsible for their ability to intercalate into bacterial membranes, bind to surface proteins, and extract lipopolysaccharides to modulate biofilm formation below their critical micellar concentration.[54] The mosaic distribution of polarity in biosurfactants is an essential property that distinguishes them from chemical surfactants with clearly separated distribution of polarity
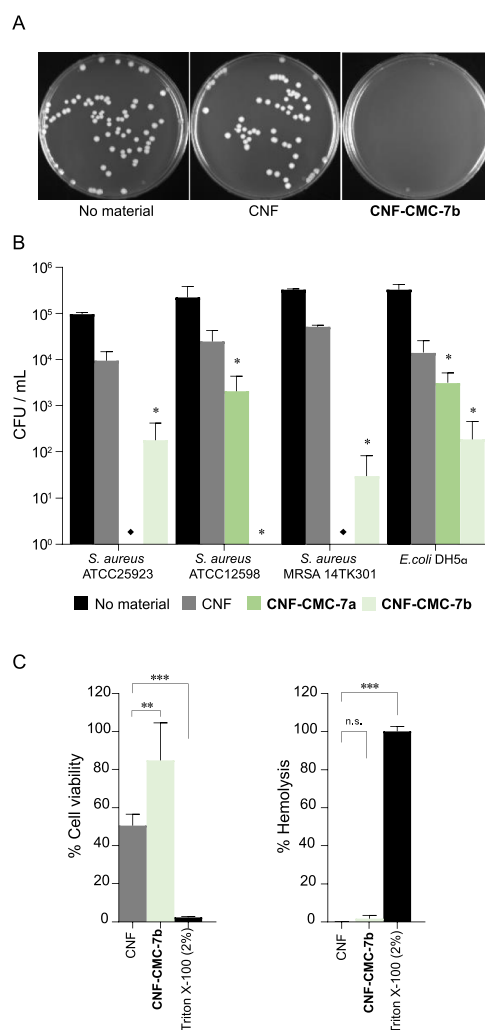
because the former cannot bind so strongly to positively charged groups in proteins and do not solubilize membranes. For **CNF-CMC-7b**, it may help to explain why fibroblasts grow well at its surface and why it does not induce significant haemolysis of red blood cells, unlike the nonionic chemical surfactant Triton-X (Figure 5C).

The anionic net charge is reported as yet another essential feature for the interactions of biosurfactants with surface proteins.[54] In this context, we tried to rule out whether **CNF-CMC-7b** significantly affected autolysins, which are the key enzymes at the surface of bacteria, responsible for cell
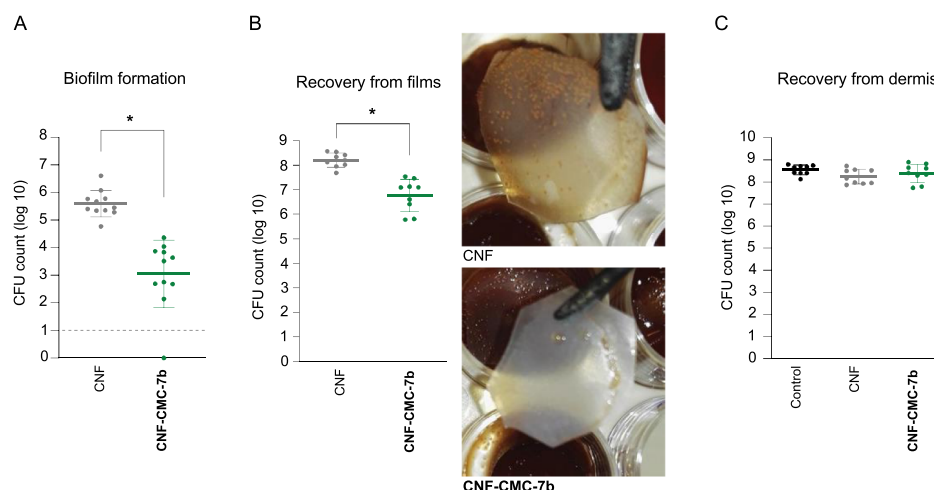
Figure 6. (A) CFU count after 24 h of UAMS-1 biofilm formation on CNF and **CNF-CMC-7b**. Statistical analysis was done using a 2-tailed independent *t*-test. **CNF-CMC-7b** showed an average reduction in recovered CFU of 2.5 log (95% CI: 1.7−3.4, $p < 0.05$, $n = 11$) compared to CNF. The dotted line indicates the detection limit; (B) CFU count from CNF and **CNF-CMC-7b** placed on infected (UAMS-1) artificial dermis. Statistical analysis was done using a 2-tailed independent *t*-test. **CNF-CMC-7b** showed an average reduction in recovered CFU of 1.4 log (95% CI: 0.9−1.9, $p < 0.05$, $n = 9$) compared to CNF. The pictures show bacterial colonization of CNF and **CNF-CMC-7b** of the material placed on top of infected artificial dermis after 24 h; (C) CFU count from artificial dermis after 24 h of UAMS-1 biofilm formation. Statistical analysis was done using a one-way ANOVA Bonferroni analysis. There was no significant difference for recovered CFU between the artificial dermises ($n = 9$).

Table 2. Antimicrobial Activity of Compounds 7a and 7b[a]

compound	MIC (μM)			
	S. aureus ATCC12598	UAMS-1	Mu50	*E. coli* DH5α
7a	60	N.D.[c]	N.D.	130
7b	15	7.4	7.4	N.A.[b]

[a]MIC = minimum inhibitory concentration. [b]N.A. = not active at the maximum concentration tested (400 μM). [c]N.D. = not determined.

Figure 7. (A) Release of ATP from *S. aureus* ATCC12598 after incubation with compounds **7a** or **7b** (100 μM) or Van (100 μM). NT = untreated cells; (B) fluorescence images depict *S. aureus* ATCC12598 or *E. coli* DH5α counts with/without treatment with compounds **7a** or **7b**, at 100 μM, for 1 h.

separation and cell wall turnover. Autolysins exist attached to the cell surface but can be released by high salt treatment and are well known to mediate cell-to-cell adherence and biofilm formation through binding to vitronectin and fibronectin.[55] Cell wall active antibiotics can interfere with autolysins, but this is usually considered a post-mortem event as they will cause killing first by inhibiting peptidoglycan synthesis.[56] Investigations in small molecules or vaccines that can modulate the activity of these autolysins are still at their infancy but have the potential to generate a new class of antimicrobial agents.[57] We found that **CNF-CMC-7b** was only 10-fold less active against a mutant strain of the Gram-positive *Lactococcus lactis* (LAC471) devoid of the AcmA autolysin than against the original *L. lactis* LAC460 strain (data not shown), suggesting that it is unlikely that release of autolysins from bacteria surfaces can be regarded as the sole mechanism of action of the films. Instead, the activity of multiple surface proteins with relevance to the integrity and biofilm-forming ability of bacteria is bound to be affected by **CNF-CMC-7b**. As an anionic surface with sugar units, **CNF-CMC-7b** could easily bind to positively charged residues and/or carbohydrate recognition sites of specific surface proteins or even indirectly modulate their activity through ion chelation in a similar fashion to what has been described for nanoparticles.[22,23,25−27] A potential suppressor of potency for **CNF-CMC-7b** in Gram-negative *E. coli* is the ability of the O-antigen to systematically hamper adhesion onto cells by completely neutralizing the negative charge carried by the supporting cell envelope.[26]
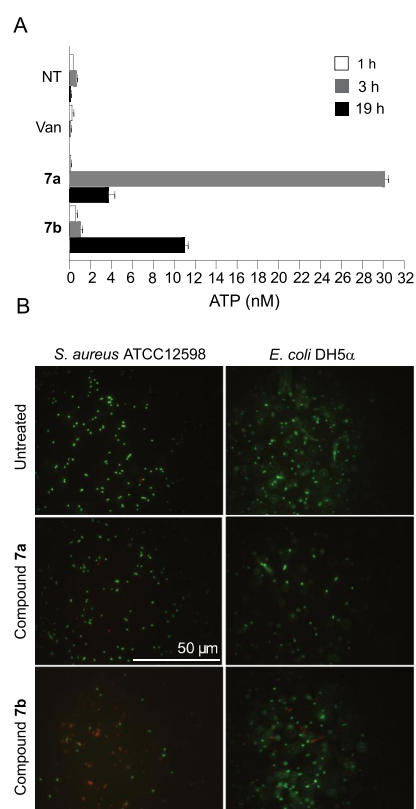
Despite these general considerations, there is yet another feature of CNF films functionalized with dehydroabietic acid derivatives that is highly relevant when discussing their potential mode of action. In line with our previous observations,[58] charge, hydrophobicity, and surface topography
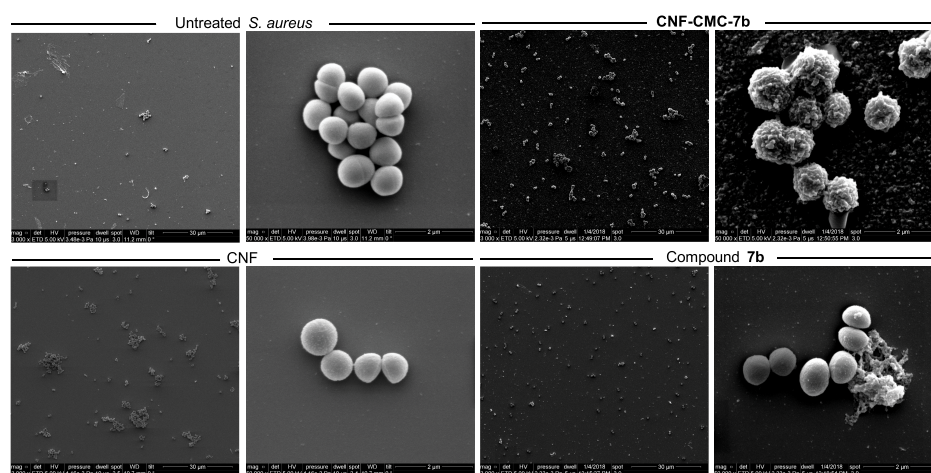
Figure 8. SEM of *S. aureus* ATCC12598 (~10^8 CFU/mL) after treatment with CNF and **CNF-CMC-7b** and **7b**, for 24 h. Left panel magnification 3000× and right panel magnification: 50,000×.

alone do not account for the bioactivity of the functionalized CNF films. However, changes in the compound bound at the surface of the film seem to be determinant. This is clearly evidenced by the fact that **CNF-CMC-7a** is weakly antimicrobial, whereas **CNF-CMC-7b**, where a β-cyclohexyl-L-alanine side chain was introduced in place of the simple methyl ester using the exact same spacer unit to CMC, is much more potent. It is therefore reasonable to speculate that the spatial orientation and binding distance of the abietane to the CMC backbone play a crucial role not only in the mosaic distribution of polarity and changes to the hydrophobicity but also in targeting specific chemical space/structures at the surface of the bacteria that trigger the antimicrobial action. The ability to fully elucidate details of the chemical space/structures will depend on future advances in techniques that are able to probe and/or model the processes occurring in the contact region between the surface and bacteria at the atomic scale. Understanding the exact nature of the interactions of surfaces based on dehydroabietic acid derivatives and CNF will undoubtedly pave the way for the development of more efficient and biocompatible antimicrobial surfaces.

CONCLUSIONS

We have successfully developed, for the first time, non-leaching, anionic, and biocompatible CNF films with the ability to resist colonization by bacteria that would lead to the undesirable establishment of a biofilm, when tested in a model that mimics the physiological conditions present in chronic wounds. By covalently coupling the dehydroabietic acid derivatives **7a** or **7b** at the surface of premade activated CNF films, we have created an interface with bacteria where the film is most likely perceived as an anionic sugar-based polymeric matrix unevenly branched with the compound, where hydrophilic and hydrophobic regions are not clearly separated. This uneven distribution of polarity combined with the spatial orientation and the binding distance of the compound to the CMC backbone at the surface of the films are likely to be the key contributors to the observed bioactivity. The activity of the films made from compound **7b** was particularly good and more relevant in Gram-positive bacteria, remaining unaffected by the presence of high protein content. This finding together with the remarkable biocompatibility of the films suggests that there is a great potential for using them

as integral parts of advanced biomaterials for human health including prosthetic implants or vascular stents, where *S. aureus* is a prevalent biofilm-forming pathogen.

EXPERIMENTAL SECTION

Compound and Film Synthesis. Dehydroabietic acid (90% purity) was purchased from Pfaltz & Bauer Inc. Acetyl chloride, iodomethane, aluminium chloride, N,N-diisopropylethylamine (DIPEA), 1-hydroxybenzotriazole hydrate (HOBt), di-t-butyl dicarbonate, cesium carbonate, sodium CMC (DS 0.70−0.85, MW ∼ 250,000), N,N-dimethylformamide (DMF), cyclohexane, ethyl acetate, hexane, heptane, methanol, and dichloromethane were acquired from Sigma-Aldrich Co. t-Butyl (3-bromopropyl)carbamate was acquired from Ega-Chemie. N-(3-Dimethylaminopropyl)-N′-ethylcarbodiimide hydrochloride (EDC·HCl), (S)-methyl 2-amino-3-cyclohexylpropanoate hydrochloride, and TFA were purchased from Fluorochem Ltd. Calcium chloride and potassium chloride were purchased from Merck & Co. Sodium bicarbonate was purchased from VWR International Oy and ethanol (Etax A, 94%) was purchased from Altia Oyj. All reagents were used without purification. Silica gel 60 F254 was used for thin layer chromatograph. Flash column chromatography was made using a Biotage high-performance flash chromatography SP4-system (Uppsala, Sweden) with a 0.1 mm path length flow cell UV detector/recorder module (fixed wavelength: 254 nm) and SNAP cartridges (25, 50 or 100 g) at 25−100 mL/min flow rate. A Vertex 70 (Bruker Optics Inc., MA, USA) instrument was used to record FTIR spectra of the compounds and films using a horizontal attenuated total reflectance (ATR) accessory (MIRacle, Pike Technology, Inc., WI, USA). Transmittance was recorded at 4 cm^{-1} resolution, between 4000 and 600 cm^{-1}, using OPUS 5.5 software (Bruker Optics Inc., MA, USA). The FTIR graphics of the films are normalized by the 1159 cm^{-1} band. Nuclear magnetic resonance (NMR) spectra of compounds were recorded on a Bruker Ascend 400 spectrometer using $CDCl_3$ with tetramethylsilane (TMS) as the internal standard. Chemical shifts are reported in parts per million (ppm) on the δ scale from TMS as an internal standard, and the coupling constants J are quoted in hertz (Hz). Exact mass analyses of the compounds were made with a Waters UPLC-ESI/QTOF-MS using a Synapt G2 HDMS (Waters, MA, USA) instrument. Compounds **3b**, **4b**, **5b**, **6a**, **6b**, **7a**, and **7b** are novel and have not been reported before.

Methyl Dehydroabietate (2a). Dehydroabietic acid **1** (0.500 g, 1.50 mmol) was dissolved in DMF (4 mL) at room temperature, and K_2CO_3 (573 mg, 4.15 mmol) and iodomethane (0.20 mL, 3.32 mmol) were added. The reaction was left under magnetic stirring for 3 h and 15 min after which it was diluted with 1 M hydrochloric acid (50 mL) and extracted with diethyl ether (3 × 75 mL). The resulting

organic phase was washed with 1 M hydrochloric acid (50 mL), a saturated solution of $NaHCO_3$ in H_2O (50 mL), water (50 mL), and brine (50 mL), dried with anhydrous Na_2SO_4, filtered, and evaporated under reduced pressure to give compound **2a** as yellow oil (0.461 g, 88%), which was used without further purification. ^{1}H NMR (400 MHz, $CDCl_3$): δ 7.16 (d, J = 8.4 Hz, 1H, aromatic-H), 7.00 (dd, J = 8.4, 1.5 Hz, 1H, aromatic-H), 6.88 (d, J = 1.6 Hz, 1H, 14-H), 3.66 (s, 3H, OCH_3), 2.77−287 (m, 3H), 2.30 (d, J = 12.4 Hz, 1H), 2.24 (dd, J = 12.8, 2.2 Hz, 1H), 1.27 (s, 3H), 1.23 (s, 3H), 1.21 (d, J = 1.2 Hz, 6H). ^{13}C NMR (101 MHz, $CDCl_3$): δ 179.2, 147.0, 145.7, 134.7, 126.9, 124.2, 123.9, 51.9, 47.7, 44.9, 38.0, 37.0, 36.7, 33.5, 30.0, 25.1, 24.0, 21.7, 18.6, 16.5. FTIR (ATR): 2927, 1721, 1247, 1174, 823 cm^{-1}. All analytical data are in agreement with literature values.[59]

Methyl *N*-(Abiet-8,11,13-trien-18-oyl) Cyclohexyl-ʟ-alaninate (2b). Dehydroabietic acid **1** (7.60 g, 22.8 mmol) was dissolved in DMF (80 mL). EDC·HCl (7.28 g, 38.0 mmol) and HOBt monohydrate (5.13 g, 38.0 mmol) were added, and the mixture was stirred for 2.25 h. β-Cyclohexyl-ʟ-alanine methyl ester hydrochloride (8.42 g, 38.0 mmol) and DIPEA (13 mL, 74.6 mmol) were added, and the mixture was stirred at room temperature for another hour. The mixture was then diluted with water (150 mL) and extracted with diethyl ether (2 × 300 mL). The resulting organic phase was washed with 1 M hydrochloric acid (200 mL), a saturated solution of $NaHCO_3$ in H_2O (200 mL), water (200 mL), and brine (50 mL) and then dried with anhydrous Na_2SO_4. The mixture was filtered and evaporated under reduced pressure. After evaporation of solvents, the white solid powder **2b** was obtained (11 g, 93%) and used without further purification. All analytical data are in agreement with literature values.[59] ^{1}H NMR (400 MHz, $CDCl_3$): δ 7.16 (d, J = 8.4 Hz, 1H, aromatic-H), 6.99 (dd, J = 8.4, 2.0 Hz, 1H, aromatic-H), 6.88 (d, J = 2.0 Hz, 1H, 14-H), 6.11 (d, J = 8.1 Hz, 1H, NH), 4.64−4.70 (m, 1H, NH(C$\underline{H}$)−), 3.71 (s, 3H, OCH_3), 2.76−2.98 (m, 3H), 2.32 (d, J = 13.2 Hz, 1H), 2.09 (dd, J = 12.4, 2.1 Hz, 1H), 1.47−1.85 (m, 17H), 1.23 (s, 3H), 1.22 (s, 3H), 1.21 (s, 3H), 0.86−1.00 (m, 3H), 0.75−0.85 (m, 3H). ^{13}C NMR (101 MHz, $CDCl_3$): δ 178.2, 174.0, 147.0, 145.8, 134.7, 127.0, 124.1, 123.9, 52.2, 50.2, 47.3, 45.8, 40.1, 38.1, 37.3, 37.2, 34.4, 33.6, 33.5, 32.4, 30.0, 26.4, 26.3, 26.1, 25.3, 24.0, 23.9, 21.1, 18.8, 16.4 cm^{-1}. FTIR (ATR): 3364, 2923, 1743, 1638, 1514, 1445, 1201, 822 cm^{-1}. UPLC−HRMS *m/z*: calcd for $C_{30}H_{46}NO_3$, 468.3478 $[M + H]^+$; found, 468.3479.

Methyl 12-Acetylabieta-8,11,13-trien-18-oate (3a). Compound **2a** (2.00 g, 6.36 mmol) was dissolved in CH_2Cl_2 (31 mL) and then AcCl (1.16 mL, 14.0 mmol) was added to the mixture. The reaction was left stirring, at 0 °C, for 5 min, after which $AlCl_3$ (1.70 g, 12.7 mmol) was added, and the mixture was left to agitate, for 45 min, at 0 °C. Then, the reaction mixture was stirred at room temperature for another hour, after which it was completed. The mixture was concentrated under reduced pressure, diluted with a saturated solution of $NaHCO_3$ in H_2O (30 mL), and extracted with diethyl ether (3 × 50 mL). The resulting organic phase was washed with a saturated solution of $NaHCO_3$ in H_2O (2 × 50 mL) and brine (50 mL), dried with Na_2SO_4, filtered, and evaporated to dryness to yield **3a** as a white solid powder (2.02 mg, 89%) that was used without further purification. ^{1}H NMR (400 MHz, $CDCl_3$): δ 7.39 (s, 1H, aromatic-H), 7.04 (s, 1H, aromatic-H), 3.67 (s, 3H, COC$\underline{H}_3$), 3.46 (sept, J = 6.8 Hz, 1H, 15-H), 2.90 (dd, J = 8.8, 4.4 Hz, 2H), 2.55 (s, 3H, OCH_3), 2.31 (d, J = 12.4 Hz, 1H), 2.22 (dd, J = 12.4, 2.4 Hz, 1H), 1.28 (s, 3H), 1.18−1.23 (m, 9H). ^{13}C NMR (101 MHz, $CDCl_3$): δ 203.4, 179.0, 146.6, 144.9, 138.8, 136.4, 127.0, 124.3, 52.0, 47.6, 44.7, 37.9, 36.9, 36.6, 30.5, 30.0, 28.7, 25.1, 24.3, 24.1, 21.5, 18.5, 16.5. FTIR (ATR): 2926, 1725, 1681, 1248, 881 cm^{-1}. UPLC−HRMS *m/z*: calcd for $C_{23}H_{33}O_3$, 357.2430 $[M + H]^+$; found, 357.2431. All analytical data are in agreement with literature values.[59]

Methyl 12-Acetyl-*N*-(abiet-8,11,13-trien-18-oyl) Cyclohexyl-ʟ-alaninate (3b). Compound **2b** (9.80 g, 21.0 mmol) was dissolved in dichloromethane (128 mL); then, AcCl (5.2 mL, 73.5 mmol) was added to the mixture. The reaction mixture was left to stir at 0 °C for 5 min, after which $AlCl_3$ (8.40 g, 63.0 mmol) was added and the mixture was left to agitate for 45 min at 0 °C. The reaction mixture was left to stir at room temperature for 2.5 h, concentrated under

reduced pressure, diluted with water (70 mL), and extracted with ethyl acetate (2 × 300 mL). The resulting organic phase was washed with water (100 mL), a saturated solution of $NaHCO_3$ in H_2O (100 mL), and brine (50 mL), dried with Na_2SO_4, filtered, and evaporated to dryness. The residue was purified by flash chromatography (SNAP 100 g, cyclohexane/ethyl acetate, gradient 8 → 80%). After evaporation of solvents, the white solid **3b** was obtained (1.67 g, 56%). ^{1}H NMR (400 MHz, $CDCl_3$): δ 7.39 (s, 1H, aromatic-H), 7.04 (s, 1H, aromatic-H), 6.09 (d, J = 8.0 Hz, 1H, NH), 4.65−4.71 (m, 1H, NH(C$\underline{H}$)−), 3.73 (s, 3H, COC$\underline{H}_3$), 3.46 (sept, J = 6.8 Hz, 1H, 15-H), 2.86−2.99 (m, 2H), 2.55 (s, 3H, OCH_3), 2.33 (d, J = 12.8 Hz, 1H), 2.11 (dd, J = 12.4, 2.0 Hz, 1H), 1.48−1.86 (m, 16H), 1.31 (s, 3H), 1.24 (s, 3H), 1.20 (dd, J = 12.4, 6.4 Hz, 7H), 0.81−1.00 (m, 3H). ^{13}C NMR (101 MHz, $CDCl_3$): δ 203.3, 178.0, 174.0, 146.6, 145.0, 138.8, 136.4, 127.1, 124.3, 52.3, 50.2, 47.2, 45.5, 40.1, 37.9, 37.1, 34.5, 33.6, 32.4, 30.6, 30.0, 28.7, 26.4, 26.3, 26.1, 25.3, 24.3, 24.1, 20.9, 18.6, 16.5 cm^{-1}. FTIR (ATR): 3360, 2923, 1744, 1641, 1517, 1260, 1201, 887. UPLC−HRMS *m/z*: calcd for $C_{32}H_{48}NO_4$, 510.3583 $[M + H]^+$; found, 510.3583.

Methyl 12-Acetoxyabieta-8,11,13-trien-18-oate (4a). Compound **3a** (1.88 g, 5.27 mmol) was dissolved in CH_2Cl_2 (7.4 mL). A solution of peracetic acid (36−40%, 12.3 mL, 199 mmol) in AcOH was added to the mixture, and the reaction mixture was left stirring at room temperature for 96 h, after which the reaction was completed. The reaction mixture was quenched by the addition of water (70 mL), and the resulting mixture was extracted with diethyl ether (4 × 70 mL). The resulting organic phases were combined and washed with a saturated solution of $NaHCO_3$ in H_2O (2 × 50 mL) and brine (50 mL) and then dried with Na_2SO_4. The mixture was filtered, evaporated under reduced pressure, and purified by flash chromatography (SNAP 50 g, *n*-heptane/ethyl acetate, 3:1). After evaporation of solvents, the yellow powder **4a** was obtained (1.73 g, 88%). ^{1}H NMR (400 MHz, $CDCl_3$): δ 6.94 (s, 1H, aromatic-H), 6.82 (s, 1H, aromatic-H), 3.66 (s, 3H, OCOC$\underline{H}_3$), 2.84−2.93 (m, 3H), 2.30 (s, 3H, OCH_3), 2.23 (dd, J = 12.4, 2.4, 1H), 2.17 (d, J = 4.0 Hz, 1H), 1.26 (s, 3H), 1.20 (s, 3H), 1.18 (t, J = 7.0 Hz, 6H). ^{13}C NMR (101 MHz, $CDCl_3$): δ 179.0, 170.0, 148.1, 146.2, 137.0, 132.9, 127.0, 117.8, 52.0, 48.0, 44.5, 37.9, 37.0, 36.6, 29.5, 27.2, 25.0, 23.1, 23.0, 21.6, 21.0, 18.5, 16.5. FTIR (ATR): 3428, 2932, 1723, 1206, 909 cm^{-1}. UPLC−HRMS *m/z*: calcd for $C_{23}H_{33}O_4$, 373.2379 $[M + H]^+$; found, 373.2383. All analytical data are in agreement with literature values.[59]

Methyl 12-Acetoxy-*N*-(abiet-8,11,13-trien-18-oyl) Cyclohexyl-ʟ-alaninate (4b). Compound **3b** (5.90 g, 11.6 mmol) was dissolved in dichloromethane (24 mL). A solution of peracetic acid (36−40%, 39 mL, 530 mmol) in AcOH was added to the mixture, and the reaction mixture was left to stir at room temperature for 72 h, after which the reaction was completed. The reaction mixture was quenched by the addition of water (100 mL), and the resulting mixture was extracted with ethyl acetate (2 × 200 mL). The resulting organic phases were combined and washed with water (100 mL), a saturated solution of $NaHCO_3$ in H_2O (3 × 100 mL), and brine (50 mL) and then dried with Na_2SO_4. The mixture was filtered and evaporated under reduced pressure to give the white solid **4b** (5.9 g, 98%) which was used without further purification. ^{1}H NMR (400 MHz, $CDCl_3$): δ 6.94 (s, 1H, aromatic-H), 6.83 (s, 1H, aromatic-H), 6.09 (d, J = 8.0 Hz, 1H, NH), 4.67 (m, 1H, NH(C$\underline{H}$)−), 3.72 (s, 3H, OCOC$\underline{H}_3$), 2.84−2.97 (m, 3H), 2.30 (s, 3H, OCH_3), 2.19−2.22 (m, 1H), 2.08 (dd, J = 12.4, 2.4 Hz, 1H), 1.48−1.81 (m, 16H), 1.29 (s, 3H), 1.23 (s, 3H), 1.17 (dd, J = 8.4, 6.9 Hz, 6H), 0.84−1.04 (m, 3H). ^{13}C NMR (101 MHz, $CDCl_3$): δ 178.1, 174.0, 170.0, 148.1, 146.2, 137.0, 132.9, 127.1, 117.8, 52.2, 50.2, 47.2, 45.4, 40.0, 38.0, 37.2, 37.2, 34.4, 33.6, 32.4, 29.4, 27.2, 26.4, 26.3, 26.1, 25.2, 23.1, 22.9, 21.0, 18.7, 16.4. FTIR (ATR): 3367, 2924, 1742, 1641, 1205, 912 cm^{-1}. UPLC−HRMS *m/z*: calcd for $C_{32}H_{48}NO_5$, 526.3532 $[M + H]^+$; found, 526.3532.

Methyl 12-Hydroxyabieta-8,11,13-trien-18-oate (5a). Compound **4a** (4.53 g, 12.2 mmol) was dissolved in MeOH (216 mL). K_2CO_3 (8.65 g, 62.6 mmol) was added, and the mixture was left to agitate at room temperature for 35 min. The reaction mixture was

filtered and concentrated under reduced pressure, diluted with water (100 mL), and extracted with ethyl acetate (3 × 150 mL). The combined organic phases were washed with water (200 mL), brine (50 mL), and dried with anhydrous Na_2SO_4. The mixture was filtered and evaporated under reduced pressure to yield the white solid **5a** (3 g, 78%), which was used without further purification. ^{1}H NMR (400 MHz, $CDCl_3$): δ 6.82 (s, 1H, aromatic-H), 6.62 (s, 1H, aromatic-H), 4.60 (s, 1H), 3.66 (s, 3H, OCH_3), 3.11 (sept, J = 6.8 Hz, 1H, 15-H), 2.78–2.83 (m, 2H), 2.16–2.23 (m, 2H), 1.33–1.84 (m, 7H), 1.26 (s, 3H), 1.23 (t, J = 6.6 Hz, 6H), 1.19 (s, 3H). ^{13}C NMR (101 MHz, $CDCl_3$): δ 179.2, 150.8, 147.9, 131.7, 127.0, 126.7, 110.8, 52.0, 47.7, 44.8, 38.0, 36.9, 36.6, 29.3, 26.8, 25.0, 22.8, 22.5, 21.9, 18.6, 16.5. FTIR (ATR): 3437, 2947, 1694, 1253, 859 cm^{-1}. UPLC−HRMS m/z: calcd for $C_{21}H_{31}O_3$, 331.2273 $[M + H]^+$; found, 331.2273. All analytical data are in agreement with literature values.[59]

Methyl-12-hydroxy-*N*-(abiet-8,11,13-trien-18-oyl) Cyclohexyl-L-alanine (5b). Compound **4b** (5.80 g, 11.0 mmol) was dissolved in MeOH (275 mL) under magnetic stirring. K_2CO_3 (7.82 g, 56.5 mmol). The mixture was left to agitate for 35 min. The reaction mixture was filtered and concentrated under reduced pressure, diluted with water (100 mL), and extracted with ethyl acetate (2 × 150 mL). The combined organic phases were washed with water (200 mL) and brine (50 mL) and dried with Na_2SO_4. The mixture was filtered and evaporated under reduced pressure to yield the yellow solid **5b** (5 g, 96%). The compound was used without further purification. ^{1}H NMR (400 MHz, $CDCl_3$): δ 6.81 (s, 1H, aromatic-H), 6.63 (s, 1H, aromatic-H), 6.10 (d, J = 8.0 Hz, 1H, NH), 4.65–4.71 (m, 1H, NH(C$\underline{H}$)−), 3.72 (s, 3H, OCH_3), 3.11 (sept, J = 6.9 Hz, 1H, 15-H), 2.76–2.89 (m, 2H), 2.21 (d, J = 12 Hz, 1H), 2.04–2.07 (m, 1H), 1.47–1.81 (m, 16H), 1.29 (s, 3H), 1.20–1.23 (m, 9H), 1.12–1.17 (m, 2H), 0.81–1.00 (m, 3H). ^{13}C NMR (101 MHz, $CDCl_3$): δ 178.3, 174.0, 150.9, 147.9, 131.8, 126.9, 126.7, 110.8, 52.2, 50.2, 47.4, 45.7, 40.1, 38.0, 37.2, 37.1, 34.4, 33.6, 32.4, 29.3, 26.8, 26.4, 26.3, 26.1, 25.2, 22.8, 22.6, 21.3, 18.8, 16.4. FTIR (ATR): 3357, 2923, 1740, 1637, 1509, 1203, 885 cm^{-1}. UPLC−HRMS m/z: calcd for $C_{30}H_{46}NO_4$, 484.3427 $[M + H]^+$; found, 484.3426.

Methyl 12-(3-Boc-aminopropoxy)abieta-8,11,13-trien-18-oate (6a). Compound **5a** (2.78 g, 8.42 mmol) was dissolved in DMF (52 mL) under magnetic stirring. *t*-Butyl (3-bromopropyl)-carbamate[58] (2.36 g, 10.1 mmol) and Cs_2CO_3 (5.49 g, 16.8 mmol) were added to the mixture that was left to agitate at room temperature for 3.5 h, after which it was filtered, diluted with water (100 mL), and extracted with ethyl acetate (3 × 100 mL). The resulting organic phase was washed with water (200 mL), a saturated solution of $NaHCO_3$ in H_2O (100 mL), and brine (50 mL) and then dried with anhydrous Na_2SO_4. The residue was purified by flash chromatography (SNAP 100 g, *n*-hexane/ethyl acetate, gradient 5 → 80%). After evaporation of solvents, colorless oil **6a** was obtained (3.8 g, 92%). ^{1}H NMR (400 MHz, $CDCl_3$): δ 6.84 (s, 1H, aromatic-H), 6.69 (s, 1H, aromatic-H), 4.90 (s, 1H, NH), 4.00 (t, J = 5.8 Hz, 2H), 3.66 (s, 3H, OCH_3), 3.35 (d, J = 6.0 Hz, 2H), 3.21 (sept, J = 6.9 Hz, 1H, 15-H), 2.79–2.83 (m, 2H), 2.21–2.26 (m, 2H), 1.95–2.01 (m, J = 5.99 Hz, 2H), 1.50–1.85 (m, 7H), 1.45 (s, 9H, $OCO(C\underline{H}_3)_3$), 1.27 (s, 3H), 1.22 (s, 3H), 1.19 (t, J = 6.8 Hz, 6H). ^{13}C NMR (101 MHz, $CDCl_3$): δ 179.1, 156.0, 154.2, 147.5, 134.4, 126.9, 126.5, 107.1, 51.9, 47.7, 44.9, 38.1, 37.2, 36.6, 29.3, 28.5, 26.6, 25.0, 23.0, 22.7, 21.9, 18.6, 16.5. FTIR (ATR): 3370, 2932, 1695, 1453, 1244, 1166, 852 cm^{-1}. UPLC−HRMS m/z: calcd for $C_{29}H_{46}NO_5$, 488.3376 $[M + H]^+$; found, 488.3376.

Methyl-12-(3-Boc-aminopropoxy)-*N*-(abiet-8,11,13-trien-18-oyl) Cyclohexyl-L-alanine (6b). Compound **5b** (3.00 g, 6.20 mmol) was dissolved in DMF (53 mL) under magnetic stirring. *t*-Butyl (3-bromopropyl)carbamate[58] (1.80 g, 7.44 mmol) and Cs_2CO_3 (4.10 g, 12.4 mmol) were added to the mixture which was left to agitate at room temperature for 4.5 h. The reaction mixture was diluted with water (100 mL) and extracted with ethyl acetate (3 × 100 mL). The resulting organic phase was washed with water (200 mL), a saturated solution of $NaHCO_3$ in H_2O (100 mL), and brine (50 mL) and then dried with anhydrous Na_2SO_4. The mixture was

filtered, evaporated under reduced pressure, and purified by flash chromatography (SNAP 100 g, eluting *n*-hexane/ethyl acetate gradient 10 → 80%). After evaporation of solvents, the white solid powder **6b** was obtained (2.4 g, 87%). ^{1}H NMR (400 MHz, $CDCl_3$): δ 6.84 (s, 1H, aromatic-H), 6.69 (s, 1H, aromatic-H), 6.08 (d, J = 8.0 Hz, 1H, CON$\underline{H}$), 4.91 (s, 1H, N$\underline{H}$Boc), 4.64–4.70 (m, 1H, NH(C$\underline{H}$)−), 4.00 (t, J = 5.8 Hz, 2H), 3.72 (s, 3H, OCH_3), 3.32–3.37 (m, J = 6.1 Hz, 2H), 3.21 (sept, J = 6.9 Hz, 1H, 15-H), 2.77–2.91 (m, 2H), 2.28 (d, J = 12.4 Hz, 1H), 2.08 (dd, J = 12.4, 2.0 Hz, 1H), 1.96–2.02 (m, 2H), 1.47–1.83 (m, 16H), 1.45 (s, 9H, $OCO(C\underline{H}_3)_3$), 1.30 (s, 3H), 1.25 (s, 3H), 1.19 (t, J = 7.2 Hz, 6H), 1.11–1.15 (m, 1H), 0.84–1.00 (m, 3H). ^{13}C NMR (101 MHz, $CDCl_3$): δ 178.1, 174.0, 156.0, 154.2, 147.5, 134.5, 126.9, 126.6, 107.0, 52.2, 50.2, 47.4, 45.8, 40.1, 38.1, 37.5, 37.2, 34.4, 33.6, 32.4, 29.4, 28.5, 26.6, 26.4, 26.3, 26.1, 25.2, 23.0, 22.7, 21.3, 18.8, 16.4. FTIR (ATR): 3304, 2923, 1752, 1165, 1062, 886 cm^{-1}. UPLC−HRMS m/z: calcd for $C_{38}H_{61}N_2O_6$, 641.4530 $[M + H]^+$; found, 641.4531.

Methyl 12-(3-Aminopropoxy)abieta-8,11,13-trien-18-oate (7a). Compound **6a** (3.80 g, 8.02 mmol) was dissolved in dichloromethane (38 mL) under magnetic stirring. TFA (6.70 mL, 86.8 mmol) was added dropwise at 0 °C. The reaction mixture was left to agitate at 0 °C for 2.7 h. After the reaction was completed, TFA and dichloromethane were evaporated under reduced pressure. The residue was diluted with ethyl acetate (200 mL) and a 1 M solution of NaOH in H_2O (100 mL). The aqueous phase was extracted with ethyl acetate (200 mL). The combined organic phase was washed with a 1 M solution of NaOH in H_2O (50 mL) and brine (50 mL) and then dried with anhydrous Na_2SO_4. The mixture was filtered and evaporated under reduced pressure. After evaporation of solvents, the white powder **7a** was obtained (2.7 g, 87%) and used without further purification. ^{1}H NMR (400 MHz, $CDCl_3$): δ 8.13 (s, 2H, NH_2), 6.83 (s, 1H, aromatic-H), 6.68 (s, 1H, aromatic-H), 4.03 (t, J = 5.8 Hz, 2H), 3.65 (s, 3H, OCH_3), 3.10–3.21 (m, 3H), 2.78–2.81 (m, 2H), 2.14–2.25 (m, 4H), 1.36–1.84 (m, 7H), 1.26 (s, 3H), 1.19 (s, 3H), 1.16 (t, J = 7.0 Hz, 6H). ^{13}C NMR (101 MHz, $CDCl_3$): δ 179.1, 154.3, 147.4, 134.5, 126.8, 126.5, 107.2, 66.0, 60.4, 51.9, 47.7, 47.7, 44.9, 39.3, 38.1, 37.2, 36.6, 32.4, 29.3, 26.6, 25.0, 22.9, 22.7, 21.9, 21.1, 18.6, 16.5, 14.2. FTIR (ATR): 2936, 1675, 1173, 1128, 834 cm^{-1}. UPLC−HRMS m/z: calcd for $C_{24}H_{38}NO_3$, 388.2852 $[M + H]^+$; found, 388.2850.

Methyl 12-(3-Aminopropoxy)-*N*-(abiet-8,11,13-trien-18-oyl) Cyclohexyl-L-alanine (7b). Compound **6b** (0.60 g, 0.94 mmol) was dissolved in dichloromethane (6 mL) under magnetic stirring. TFA (1.0 mL, 13 mmol) was added dropwise at 0 °C. The reaction mixture was left to agitate at 0 °C for 2 h. After the reaction was completed, TFA and dichloromethane were evaporated under reduced pressure. The residue was diluted with ethyl acetate (70 mL) and a 1 M solution of NaOH in H_2O (30 mL). The aqueous phase was extracted with ethyl acetate (2 × 50 mL). The combined organic phase was washed with a 1 M solution of NaOH in H_2O (50 mL) and brine (50 mL) and then dried with anhydrous Na_2SO_4. The mixture was filtered and concentrated under reduced pressure. After evaporation of solvents, the light pink solid **7b** was obtained (0.479 g, 94%) and used without further purification. ^{1}H NMR (400 MHz, $CDCl_3$): δ 6.83 (s, 1H, aromatic-H), 6.69 (s, 1H, aromatic-H), 6.10 (d, J = 8.4 Hz, 1H, N$\underline{H}$), 5.62 (s, 2H, NH_2), 4.64–4.69 (m, 1H, NH(C$\underline{H}$)−), 4.03 (t, J = 5.8 Hz, 2H), 3.72 (s, 3H, OCH_3), 3.07–3.20 (m, 3H), 2.77–2.90 (m, 2H), 2.27 (d, J = 12.8 Hz, 1H), 2.04–2.11 (m, 3H), 1.44–1.80 (m, 16H), 1.29 (s, 3H), 1.23 (s, 3H), 1.17 (t, J = 7.0 Hz, 6H), 0.84–1.00 (m, 3H). ^{13}C NMR (101 MHz, $CDCl_3$): δ 178.2, 174.0, 154.0, 147.5, 134.6, 127.2, 126.7, 107.4, 66.0, 52.2, 50.2, 47.3, 45.8, 40.1, 38.8, 38.1, 37.4, 37.2, 34.4, 33.6, 32.4, 29.3, 26.6, 26.4, 26.3, 26.1, 25.2, 22.9, 22.7, 21.2, 18.7, 16.4 FTIR (ATR): 3362, 2923, 1741, 1500, 886 cm^{-1}. UPLC−HRMS m/z: calcd for $C_{33}H_{53}N_2O_4$, 541.4005 $[M + H]^+$; found, 541.4004.

Preparation of CNF Films. Never-dried birch kraft pulp was used to prepare CNF films, as reported previously.[58] The pulp dispersion was obtained by disintegrating using a high-pressure fluidizer (Microfluidics, M-110Y, Microfluidics Int. Co., Newton, MA) and

circulated for 6 passes. Prior to disintegration, the pulp had not been chemically or enzymatically pretreated but washed into sodium form in order to control the counter-ion type. Briefly, to prepare free-standing films, 100 mL of CNF dispersion diluted to 0.85% was filtered through a Sefar Nitex polyamine filament fabric for 30 min at 2.5 bar. The pore size of the fabric was 10 μm. The formed film was then hot-pressed for 2 h at 100 °C and at 1800 kg/cm^2 pressure, using a Carver Laboratory Press (Fred S. Carver Inc.). More detailed information about free-standing CNF films and their production can be found elsewhere.[33] The CNF films were stored at standard conditions (23 °C, 50% RH) and cut according to the amounts needed for each procedure.

Functionalization of CNF Films. The reaction was carried out on a round-bottomed reaction flask, with magnetic stirring, using 5 cm diameter CNF films immersed in an aqueous solution (75 mL) of CaCl$_2$/NaHCO$_3$ (0.05 M/0.01 M) and Na—CMC (270 mg), at 80 °C, for 4 h, after which the reaction mixture was poured out from the flask and the CNF circle was washed, under magnetic stirring, with deionized water (150 mL, 10 min), a 0.1 M solution of CH$_3$COOH in H$_2$O (75 mL, 10 min), deionized water (150 mL, 10 min), a 0.4% solution of NaHCO$_3$ in H$_2$O (75 mL, 1 h), and deionized water (150 mL, 10 min), dried overnight at 103 °C, and pressed between 2 carton sheets. After the carboxymethylation, one 5 cm diameter CNF film was added to a round-bottomed flask containing EDC·HCl (0.02 M), HOBt (0.02 M), and Etax A (60 mL) and left under magnetic stirring at room temperature for 1 h. Compounds **7a** or **7b** (0.02 M) and DIPEA (0.04 M) were added, and the mixture was left to agitate at room temperature for additional 24 h, after which it was poured out of the reaction flask, and the CNF film was rinsed with Etax A (20 mL) and then washed 4 times, under magnetic stirring, with deionized water (150 mL × 4, 10 min each washing), recovered, placed between 2 carton sheets, and left in an oven to dry overnight at 103 °C.

Mass Analysis. **CNF-CMC-7b** was directly compared to **CNF-CMC**, unmodified CNF and compound **7b** powder. Samples of **CNF-CMC-7b** were analyzed from different production batches to confirm reproducibility. CNF films were cut to an approximate size of 1 cm^2 and inserted directly into the sample holder. To analyze **7b**, a small piece of double-sided carbon tape (∼1 cm^2) was attached to an aluminum block and a small amount of the compound was added to the exposed adhesive surface. After light pressing with a spatula, excess powder was removed by careful tipping and a gentle stream of nitrogen. Surface analyses were carried out on a ToF-SIMS 5 mass spectrometer (IONTOF GmbH, Germany) using a 30 keV Bi$_3$$^+$ analysis beam. An electron flood gun was used for charge compensation. CNF films were analyzed using spectrometry mode data acquired from a surface area of 500 × 500 μm^2 at 512 × 512 pixels in positive and negative ionization modes. Spectra were acquired at a cycle time of 150 μs. An ion dose of 5 × 10^{11} ions/cm^2 was maintained in order to stay below the static SIMS limit. The powder sample was analyzed over a smaller target area of 250 × 250 μm^2 at 256 × 256 pixels and with a lower dose of 1 × 10^{11} ions/cm^2. Data analysis was carried out on SurfaceLab software version 7 (IONTOF GmbH, Germany).

Water Contact Angle. The water contact angle was measured using a CAM 2000 (KSV Instruments Ltd., Finland). CNF films (1 × 1 cm^2) were taped onto silica wafers, and a 6.5 μL droplet of Milli-Q water was used for measuring. Built-in software analyzed the shape of the droplet and obtained the water contact angle value using the Young−Laplace equation. The static water contact angle was measured for 60 s, but because of water droplets causing bending of the CNF films, the water contact angles at 5 and 30 s are reported. At least four measurements were taken for each sample, and mean values are reported.

Streaming Current Measurements. The streaming current was measured, at varying pressures (0−200 mbar), across streaming channels formed by identically treated sample surfaces using the microslit electrokinetic setup. Circular samples with a diameter of 15 mm were punched out from unmodified or modified CNF films and fixed at movable stamps of a flow cell with a variable channel width. The distance between the sample surfaces was set to 60 μm. The

measurements were performed as a function of the solution pH starting in the alkaline pH range. For each pH condition tested, the samples were equilibrated for about 40 min prior to measurement. The electrolyte solutions used for the streaming current measurements were prepared from vacuum-degassed deionized water (Milli-Q Integral 3, Merck Millipore, Germany) by addition and/or appropriate dilution of 0.1 M stock solutions.

X-ray Photoelectron Spectroscopy. Surface chemical analysis of CNF films (1 × 1 cm^2) was performed with a Kratos Analytical AXIS Ultra electron spectrometer with monochromatic A1 Kα irradiation at 100 W. Prior to measuring, the films were extracted in acetone to remove impurities. CasaXPS software was used for data analysis, and for the carbon regions, a specific four-component fitting routine tailored for a cellulosic specimen was used.[60] Low resolution survey scans were used to determine the elemental surface composition, and high resolution carbon C 1s and oxygen O 1s regions were applied for a more detailed chemical evaluation. Nitrogen contents were evaluated using long regional N 1s scan that were recorded with survey resolution so that they could be incorporated into survey quantifications. Three locations of each sample were measured, and pure cellulose filter paper (Whatman) was used as an in situ reference. The nominal analysis area was 300 × 700 μm^2. Surface coverage was calculated by dividing the measured N or C−C content with theoretical N or C−C content, respectively. The theoretical N and C−C contents are based on the respective amounts of nitrogen and carbon atoms with bonds to only other carbon or hydrogen atoms in the chemical structure of the compounds.

Microbiology. *S. aureus* ATCC12598, *S. aureus* ATCC25923, *S. aureus* MRSA 14TK3013, and *E. coli* DH5α were grown on Luria-Bertani (LB, 10 g/L tryptone, 5 g/L yeast extract, 5 g/L NaCl) agar or in broth with shaking at 37 °C. *L. lactis* LAC460 and LAC471 were grown in M17 media supplemented with 0.5% glucose. Overnight *S. aureus* and *E. coli* cultures were serially diluted in one-fourth Ringer solution (CaCl$_2$ 0.12 g/L, KCl 0.105 g/L, NaHCO$_3$ 0.05 g/L, NaCl 2.25 g/L), and overnight lactococcal cultures were diluted in minimal media SD3 without sugar to certain concentrations for corresponding assays. UAMS-1 and Mu50 were subcultured on Mueller−Hinton agar (Lab M Limited, Lancashire, UK), at 37 °C, under aerobic conditions. Liquid cultures were grown in Mueller−Hinton broth (Lab M Limited), at 37 °C, under aerobic conditions.

Antimicrobial Activity of the Films. CNF films (5 cm diameter) were cut into pieces (1 × 1 cm^2) and incubated in 1.35 mL of bacterial suspensions with ∼10^5 CFU/mL, for 24 h, at 37 °C and with shaking at 160 rpm for *E. coli* and *S. aureus* and at 30 °C with shaking at 120 rpm, for *L. lactis*. Afterward, numeration of viable bacteria was done.

Atomic Force Microscopy. Modified and unmodified free-standing CNF films were imaged with a Nanoscope V MultiMode scanning probe microscope (Corporation, Billerica, Massachusetts, USA). The images were recorded with a tapping mode in air using silicon cantilevers (NSC15/AIBS, MicroMasch, Tallinn, Estonia). According to the manufacturer, the radius of the tip was <10 nm. At least three places for each sample were imaged.

Antimicrobial Activity of Compounds 7a and 7b. *S. aureus* ATCC12598 and *E. coli* DH5α were cultured with various concentrations of compounds **7a** or **7b**. Honeycomb microtiter plate wells were filled with 300 μL of LB media with 0.1% of overnight culture. The final concentrations used for *S. aureus* and *E. coli* were 10, 20, 30, 40, 50, and 60 μM. Plates were incubated in Bioscreen C (Labsystems, Helsinki, Finland), at 37 °C, with constant shaking. Optical density was measured every hour with a wideband filter (420−580 nm). All MIC determinations were done in triplicate, and MIC was defined as the lowest concentration of compound for which the OD values of all three parallels were below 0.2, in 12 h.

Measurement of ATP Efflux from *S. aureus* ATCC12598 Following Treatment with Compounds 7a and 7b. The efflux of ATP from *S. aureus* ATCC12598 was measured using luciferin−luciferase bioluminescence assay. Overnight culture of *S. aureus* was collected and resuspended in one-fourth Ringer solution to ∼10^9 CFU/mL. One milliliter of cell suspension was incubated with

compounds **7a** or **7b** at a final concentration of 100 μM, for 1 h at 37 °C, with shaking. After the incubation, 10 μL of cell free supernatants was added to 100 μL of reaction solution in bioluminescence assay, according to supplier's protocol (Thermo Fisher, Waltham, MA, USA). Bioluminescence was measured in a EnSprie multimode plate reader (PerkinElmer, Waltham, MA, USA).

Scanning Electron Microscopy. Overnight culture of *S. aureus* was diluted in one-fourth Ringer solution to ~10^8 CFU/mL and incubated with CNF films (1 × 1 cm^2), for 24 h, or with compound **7b** for 1 h, at 37 °C, with shaking. The cells were then collected by centrifugation (5000*g*, 5 min), at 22 °C, resuspended in 0.1 M phosphate buffer (pH 7.4), and fixed in 2% glutaraldehyde, for 2 h. Cell samples subject to scanning electron microscopy (SEM) were prepared according to standard protocol for the air drying technique.[61] After dehydration into absolute ethanol, specimens were dried using Fluka hexamethyldisilazane, mounted into aluminium stubs, coated with platinum, and examined under an FEI Quanta 250 field emission gun scanning electron microscope at an accelerating voltage of 5 kV (Electron Microscopy Unit, University of Helsinki, Finland).

Biofilms. The *S. aureus* UAMS-1 strain was used for all biofilm experiments. CNF and **CNF-CMC-7b** were cut into circles with a 0.5 cm diameter and placed in a flat-bottomed 48-well microtiter plate (Greiner Bio-One, Kremsmünster, Austria). The samples were submerged in 400 μL of Mueller–Hinton broth and inoculated with 10^4 CFU *S. aureus* UAMS-1 (obtained from an overnight culture). After 4 h incubation at 37 °C, medium was removed, the samples were washed with 400 μL of PS (0.9% w/v NaCl), and a new medium was added. After another 20 h, the medium was removed; the samples were moved to a new well, and washed with 400 μL PS. After washing, the biofilm was collected by 3 cycles of vortexing and sonication for 30 s. The number of CFU was determined through plating.

Artificial Dermis Experiments. The artificial dermis is composed of two layers and was prepared, as previously described.[62] The artificial dermis was placed into a flat-bottomed 24-well microtiter plate (Greiner Bio-One, Kremsmünster, Austria). The medium was composed of Bolton Broth (Oxoid, Basingstoke, UK) containing 50% plasma (Sigma-Aldrich), 5% freeze–thaw laked horse blood, and 0.5 U/mL heparin (Calbiochem, San Diego, USA). Medium (500 μL) was pipetted on top of the artificial dermis, and subsequently, 10 μL of an overnight culture of *S. aureus* UAMS-1 (containing approx 10^4 CFU) was added. The medium was added to the wells to a final volume of 1 mL by pipetting around the artificial dermis to avoid dehydration. CNF and **CNF-CMC-7b** were cut to fully cover the expanded artificial dermis, placed on top of the artificial dermis, and pushed onto the artificial dermis until they stuck to the surface. The plate was cultivated at 37 °C for 24 h after which the material was taken off and washed with 1 mL of PS. The artificial dermis was collected in a tube containing 10 mL of PS. Biofilms were collected by alternating vortexing and sonication for 30 s 3 times. The CFU counts were determined by plating. Verification of the normal distribution of the data was done using the Shapiro–Wilk test. The log 10 values for the CFU counts between groups were compared by an independent sample *t*-test for the material data. The artificial dermis data was analyzed using a one-way analysis of variance (ANOVA) Bonferroni analysis. The statistical analyses were carried out with SPSS version 25 (SPSS Inc., Chicago, USA).

Determination of MIC on UAMS-1 and Mu50 Strains. The MIC was determined according to the EUCAST broth microdilution guidelines.[63] The MIC was determined in triplicate using a flat-bottomed 96 well microtiter plate (Greiner Bio-One, Kremsmünster, Austria) using Mueller–Hinton broth as growth medium. The tested concentrations ranged from 0.25 to 128 μg/mL. The overnight planktonic cultures were adjusted to obtain a final inoculum of 5 × 10^5 CFU/mL in the wells. Plates were incubated at 37 °C for 24 h, and optical density at 590 nm was determined using an Envision plate reader (PerkinElmer, Waltham, MA, USA). The MIC values were determined as the lowest concentration of **7b** at which growth was completely inhibited.

Blood Hemolysis. Whole blood (1.0 mL) collected from healthy human donors (Scottish National and Transfusion Services, Scotland, Sample Governance Submission 19~17) was pipetted into an Eppendorf tube and centrifuged at 500*g*, for 5 min in an Heraeus Megafuge 16 (Thermo Scientific), and the levels of hematocrit (red, lower layer) and plasma (yellowish, upper layer) were marked with pen on the Eppendorf tube. The upper fraction (plasma) was gently removed via a micropipettor and replaced with a cold 150 mM solution of NaCl in Milli-Q to the marked line. The Eppendorf tube was closed and inverted six times to gently disperse the lower fraction (hematocrit) in the NaCl solution. The mixture was subsequently centrifuged at 500*g*, for 5 min, and again the supernatant solution was removed and replaced with a cold 150 mM solution of NaCl in water to further wash the erythrocytes. The supernatant was again aspirated and replaced with 1× phosphate-buffered saline (PBS) at pH 7.4, followed with six tube inversions to uniformly mix the erythrocytes with the PBS. The erythrocytes were then diluted in a 1:50 ratio in 50 mL falcons (Corning Inc. Life Sciences) with sterile PBS after which 12 mm diameter circles of plain CNF and **CNF-CMC-7b** films were individually placed at the bottom of a 24-well plate (Corning Inc. Life Sciences) and washed with sterile PBS. The erythrocyte dilution (2 mL) was placed into each corresponding well, 2 mL of the dilution was placed in empty wells, and 200 μL of 20% Triton X-100 and 1800 μL of PBS were placed in the last wells as control. All wells were visually inspected which should be turbid and settle if left undisturbed. The plates were incubated for 1 h, at 37 °C, in a 5% CO$_2$ atmosphere in a MCO-170M multi gas incubator (Panasonic Biomedical), and 1 mL of samples from the wells were subsequently collected in sterile 1.5 mL Eppendorf tubes and centrifuged at 500*g* for 5 min to pellet the intact erythrocytes. Supernatant from the Eppendorf tubes (200 μL) was transferred to a 96-well plate (PerkinElmer Inc.) and the absorbance was measured at 415 nm, using a Flex Station 3 multi-mode microplate reader (Molecular Devices). The negative background absorbance was subtracted from all samples and each value normalized to the positive Triton-treated control (100% lysis) to calculate percent hemolysis.

Cell Viability. Human skin fibroblasts were cultured in a 75 cm^2 flask (Corning Inc. Life Sciences) in Dulbecco's modified Eagle's medium (HyClone) supplemented with 10% fetal bovine serum, 1% sodium pyruvate, 1% nonessential amino acids, 1% L-glutamine, penicillin (100 IU/mL), and streptomycin (100 mg/mL) (all from HyClone). The cultures were maintained in a Heracell 150i incubator (Thermo Fisher Scientific) in an atmosphere of 5% CO$_2$ and 95% relative humidity. The growth medium was changed every other day until the time of use. CNF and **CNF-CMC-7b** films were cut into 12 mm diameter circles, individually placed at the bottom of a 24-well plate (Corning Inc. Life Sciences), and washed with sterile PBS. Subsequently, the fibroblasts were detached using a trypsin–PBS–EDTA solution, and 4 × 10^4 human fibroblasts were placed on top of the materials in the 24-well plate. The cells were allowed to attach and incubate with the films, for 72 h, with the medium replaced every other day. After the incubation period, the medium was aspirated and the cells and materials were washed twice with fresh sterile PBS. Then, 1 mL of CellTiter-Glo reagent assay (Promega Corporation) was added to each well according to the manufacturer's instructions. Luminescence was measured using a Varioskan Lux (Thermo Fisher Scientific). The luminescence of the sample wells was compared with positive (PBS) and negative (2% Triton X-100) controls. All assays were carried out at least in quadruplicate.

■ ASSOCIATED CONTENT

ⓢ Supporting Information

The Supporting Information is available free of charge at https://pubs.acs.org/doi/10.1021/acsabm.0c00203.

> NMR spectra of compounds **2b**, **3b**, **4b**, **5b**, **6a**, **6b**, **7a**, and **7b**; ToF-SIMS analysis (full spectra); AFM images (CNF, **CNF-CMC-7b**) (PDF)

AUTHOR INFORMATION

Corresponding Authors

Monika Österberg − *Department of Bioproducts and Biosystems, Aalto University, FI-00076 Aalto, Finland;* ● orcid.org/0000-0002-3558-9172; Email: monika.osterberg@aalto.fi

Vânia M. Moreira − *Drug Research Program, Division of Pharmaceutical Chemistry and Technology, Faculty of Pharmacy, University of Helsinki, FI-00014 Helsinki, Finland; Strathclyde Institute of Pharmacy and Biomedical Sciences, University of Strathclyde, G4 0RE Glasgow, U.K.;* ● orcid.org/0000-0001-6169-5035; Email: vmoreira@ff.uc.pt

Authors

Ghada Hassan − *Drug Research Program, Division of Pharmaceutical Chemistry and Technology, Faculty of Pharmacy, University of Helsinki, FI-00014 Helsinki, Finland*

Nina Forsman − *Department of Bioproducts and Biosystems, Aalto University, FI-00076 Aalto, Finland*

Xing Wan − *Department of Microbiology, Faculty of Agriculture and Forestry, University of Helsinki, FI-00014 Helsinki, Finland*

Leena Keurulainen − *Drug Research Program, Division of Pharmaceutical Chemistry and Technology, Faculty of Pharmacy, University of Helsinki, FI-00014 Helsinki, Finland*

Luis M. Bimbo − *Strathclyde Institute of Pharmacy and Biomedical Sciences, University of Strathclyde, G4 0RE Glasgow, U.K.;* ● orcid.org/0000-0002-8876-8297

Susanne Stehl − *Leibniz Institute of Polymer Research Dresden, Max Bergmann Centre for Biomaterials Dresden, 01069 Dresden, Germany*

Frits van Charante − *Laboratory of Pharmaceutical Microbiology, Ghent University, 9000 Gent, Belgium*

Michael Chrubasik − *EPSRC Future Manufacturing Research Hub for Continuous Manufacturing and Advanced Crystallisation, Strathclyde Institute of Pharmacy and Biomedical Sciences, University of Strathclyde, Technology and Innovation Centre, G1 1RD Glasgow, U.K.; National Physical Laboratory, TW11 0LW Teddington, U.K.*

Aruna S. Prakash − *EPSRC Future Manufacturing Research Hub for Continuous Manufacturing and Advanced Crystallisation, Strathclyde Institute of Pharmacy and Biomedical Sciences, University of Strathclyde, Technology and Innovation Centre, G1 1RD Glasgow, U.K.; National Physical Laboratory, TW11 0LW Teddington, U.K.*

Leena-Sisko Johansson − *Department of Bioproducts and Biosystems, Aalto University, FI-00076 Aalto, Finland*

Declan C. Mullen − *Strathclyde Institute of Pharmacy and Biomedical Sciences, University of Strathclyde, G4 0RE Glasgow, U.K.*

Blair F. Johnston − *EPSRC Future Manufacturing Research Hub for Continuous Manufacturing and Advanced Crystallisation, Strathclyde Institute of Pharmacy and Biomedical Sciences, University of Strathclyde, Technology and Innovation Centre, G1 1RD Glasgow, U.K.; National Physical Laboratory, TW11 0LW Teddington, U.K.*

Ralf Zimmermann − *Leibniz Institute of Polymer Research Dresden, Max Bergmann Centre for Biomaterials Dresden, 01069 Dresden, Germany;* ● orcid.org/0000-0003-4256-0754

Carsten Werner − *Leibniz Institute of Polymer Research Dresden, Max Bergmann Centre for Biomaterials Dresden, 01069 Dresden, Germany;* ● orcid.org/0000-0003-0189-3448

Jari Yli-Kauhaluoma − *Drug Research Program, Division of Pharmaceutical Chemistry and Technology, Faculty of Pharmacy, University of Helsinki, FI-00014 Helsinki, Finland;* ● orcid.org/0000-0003-0370-7653

Tom Coenye − *Laboratory of Pharmaceutical Microbiology, Ghent University, 9000 Gent, Belgium*

Per E. J. Saris − *Department of Microbiology, Faculty of Agriculture and Forestry, University of Helsinki, FI-00014 Helsinki, Finland*

Complete contact information is available at:
https://pubs.acs.org/10.1021/acsabm.0c00203

Author Contributions

G.H. and L.K. were responsible for compound synthesis and characterization as well as for CNF functionalization. N.F. made the unmodified CNF films. N.F. and M.Ö. were responsible for film analysis including CA measurements and XPS and FTIR data analysis. L.-S.J. performed the XPS analysis of films. X.W. and P.E.J.S. were responsible for microbiological analysis of compound and surfaces, including SEM experiments. L.M.B. was responsible for human fibroblast viability and hemolysis testing. S.S., R.Z., and C.W. were responsible for streaming current measurements. F.v.C. and T.C. were responsible for biofilms and artificial dermis experiments as well as for antimicrobial testing of compounds on UAMS-1 and Mu50 strains. M.C., A.S.P., D.C.M., and B.F.J. were responsible for ToF-SIMS analysis including data analysis. J.Y.-K. revised the manuscript. V.M.M. and M.Ö. designed and planned all experiments and supervised the work. G.H., N.F., X.W., L.M.B., F.v.C., A.S.P., D.C.M., R.Z., and V.M.M. wrote the manuscript. All authors have given approval to the final version of the manuscript.

■ REFERENCES

(1) Koo, H.; Allan, R. N.; Howlin, R. P.; Stoodley, P.; Hall-Stoodley, L. Targeting microbial biofilms: current and prospective therapeutic strategies. *Nat. Rev. Microbiol.* **2017**, *15*, 740−755.

(2) Mas-Moruno, C.; Su, B.; Dalby, M. J. Multifunctional Coatings and Nanotopographies: Toward Cell Instructive and Antibacterial Implants. *Adv. Healthcare Mater.* **2019**, *8*, 1801103.

(3) Banerjee, I.; Pangule, R. C.; Kane, R. S. Antifouling coatings: recent developments in the design of surfaces that prevent fouling by proteins, bacteria, and marine organisms. *Adv. Mater.* **2011**, *23*, 690−718.

(4) Hasan, J.; Crawford, R. J.; Ivanova, E. P. Antibacterial surfaces: the quest for a new generation of biomaterials. *Trends Biotechnol.* **2013**, *31*, 295−304.

(5) Tuson, H. H.; Weibel, D. B. Bacteria−surface interactions. *Soft Matter* **2013**, *9*, 4368−4380.

(6) Bormashenko, E. Physics of pre-wetted, lubricated and impregnated surfaces: a review. *Philos. Trans. R. Soc., A* **2019**, *377*, 20180264.

(7) Modaresifar, K.; Azizian, S.; Ganjian, M.; Fratila-Apachitei, L. E.; Zadpoor, A. A. Bactericidal effects of nanopatterns: A systematic review. *Acta Biomater.* **2019**, *83*, 29−36.

(8) Hook, A. L.; Chang, C.-Y.; Yang, J.; Luckett, J.; Cockayne, A.; Atkinson, S.; Mei, Y.; Bayston, R.; Irvine, D. J.; Langer, R.; Anderson, D. G.; Williams, P.; Davies, M. C.; Alexander, M. R. Combinatorial discovery of polymers resistant to bacterial attachment. *Nat. Biotechnol.* **2012**, *30*, 868−875.

(9) Mikulskis, P.; Hook, A.; Dundas, A. A.; Irvine, D.; Sanni, O.; Anderson, D.; Langer, R.; Alexander, M. R.; Williams, P.; Winkler, D. A. Prediction of broad-spectrum pathogen attachment to coating materials for biomedical devices. *ACS Appl. Mater. Interfaces* **2018**, *10*, 139−149.

(10) Jakobsen, T. H.; Eickhardt, S. R.; Gheorghe, A. G.; Stenqvist, C.; Sønderholm, M.; Stavnsberg, C.; Jensen, P. Ø.; Odgaard, A.; Whiteley, M.; Moser, C.; Hvolris, J.; Hougen, H. P.; Bjarnsholt, T. Implants induce a new niche for microbiomes. *APMIS* **2018**, *126*, 685−692.

(11) Penesyan, A.; Nagy, S. S.; Kjelleberg, S.; Gillings, M. R.; Paulsen, I. T. Rapid microevolution of biofilm cells in response to antibiotics. *npj Biofilms Microbiomes* **2019**, *5*, 34.

(12) Crabbé, A.; Jensen, P. Ø.; Bjarnsholt, T.; Coenye, T. Antimicrobial Tolerance and Metabolic Adaptations in Microbial Biofilms. *Trends Microbiol.* **2019**, *27*, 850−863.

(13) Percival, S. L.; Suleman, L.; Vuotto, C.; Donelli, G. Healthcare-associated infections, medical devices and biofilms: risk, tolerance and control. *J. Med. Microbiol.* **2015**, *64*, 323−334.

(14) Flynn, P. B.; Gilmore, B. F. Understanding plasma biofilm interactions for controlling infection and virulence. *J. Phys. D: Appl. Phys.* **2018**, *51*, 263001.

(15) Hosseinidoust, Z.; Olsson, A. L. J.; Tufenkji, N. Going viral: Designing bioactive surfaces with bacteriophage. *Colloids Surf., B* **2014**, *124*, 2−16.

(16) Ren, W.; Cheng, W.; Wang, G.; Liu, Y. Developments in antimicrobial polymers. *J. Polym. Sci., Part A: Polym. Chem.* **2017**, *55*, 632−639.

(17) Diaz-Gomez, L.; Concheiro, A.; Alvarez-Lorenzo, C. Functionalization of titanium implants with phase-transited lysozyme for gentle immobilization of antimicrobial lysozyme. *Appl. Surf. Sci.* **2018**, *452*, 32−42.

(18) Mannoor, M. S.; Tao, H.; Clayton, J. D.; Sengupta, A.; Kaplan, D. L.; Naik, R. R.; Verma, N.; Omenetto, F. G.; McAlpine, M. C. Graphene-based wireless bacteria detection on tooth enamel. *Nat. Commun.* **2012**, *3*, 763.

(19) Henriques, P. C.; Borges, I.; Pinto, A. M.; Magalhães, F. D.; Gonçalves, I. C. Fabrication and antimicrobial performance of surfaces integrating graphene-based materials. *Carbon* **2018**, *132*, 709−732.

(20) Pelaz, B.; Alexiou, C.; Alvarez-Puebla, R. A.; Alves, F.; Andrews, A. M.; Ashraf, S.; Balogh, L. P.; Ballerini, L.; Bestetti, A.; Brendel, C.; Bosi, S.; Carril, M.; Chan, W. C. W.; Chen, C.; Chen, X.; Chen, X.; Cheng, Z.; Cui, D.; Du, J.; Dullin, C.; Escudero, A.; Feliu, N.; Gao, M.; George, M.; Gogotsi, Y.; Grünweller, A.; Gu, Z.; Halas, N. J.; Hampp, N.; Hartmann, R. K.; Hersam, M. C.; Hunziker, P.; Jian, J.; Jiang, X.; Jungebluth, P.; Kadhiresan, P.; Kataoka, K.; Khademhosseini, A.; Kopeček, J.; Kotov, N. A.; Krug, H. F.; Lee, D. S.; Lehr, C.-M.; Leong, K. W.; Liang, X.-J.; Ling Lim, M.; Liz-Marzán, L. M.; Ma, X.; Macchiarini, P.; Meng, H.; Möhwald, H.; Mulvaney, P.; Nel, A. E.; Nie, S.; Nordlander, P.; Okano, T.; Oliveira, J.; Park, T. H.; Penner, R. M.; Prato, M.; Puntes, V.; Rotello, V. M.; Samarakoon, A.; Schaak, R. E.; Shen, Y.; Sjöqvist, S.; Skirtach, A. G.; Soliman, M. G.; Stevens, M. M.; Sung, H.-W.; Tang, B. Z.; Tietze, R.; Udugama, B. N.; VanEpps, J. S.; Weil, T.; Weiss, P. S.; Willner, I.; Wu, Y.; Yang, L.; Yue, Z.; Zhang, Q.; Zhang, Q.; Zhang, X.-E.; Zhao, Y.; Zhou, X.; Parak, W. J. Diverse Applications of Nanomedicine. *ACS Nano* **2017**, *11*, 2313−2381.

(21) Yuan, H.; Liu, Z.; Liu, L.; Lv, F.; Wang, Y.; Wang, S. Cationic Conjugated Polymers for Discrimination of Microbial Pathogens. *Adv. Mater.* **2014**, *26*, 4333−4338.

(22) Feng, Z. V.; Gunsolus, I. L.; Qiu, T. A.; Hurley, K. R.; Nyberg, L. H.; Frew, H.; Johnson, K. P.; Vartanian, A. M.; Jacob, L. M.; Lohse, S. E.; Torelli, M. D.; Hamers, R. J.; Murphy, C. J.; Haynes, C. L. Impacts of Gold Nanoparticle Charge and Ligand Type on Surface Binding and Toxicity to Gram-Negative and Gram-Positive Bacteria. *Chem. Sci.* **2015**, *6*, 5186−5196.

(23) Richards, S.-J.; Isufi, K.; Wilkins, L. E.; Lipecki, J.; Fullam, E.; Gibson, M. I. Multivalent Antimicrobial Polymer Nanoparticles Target Mycobacteria and Gram-Negative Bacteria by Distinct Mechanisms. *Biomacromolecules* **2018**, *19*, 256−264.

(24) Boucard, J.; Boudjemaa, R.; Steenkeste, K.; Jacqueline, C.; Stephant, N.; Lefèvre, F.-X.; Laurent, A. D.; Lartigue, L.; Hulin, P.; Nedellec, S.; Fontaine-Aupart, M.-P.; Ishow, E. Phosphonic Acid Fluorescent Organic Nanoparticles for High-Contrast and Selective Staining of Gram-Positive Bacteria. *ACS Omega* **2018**, *3*, 17392−17402.

(25) Pillai, P. P.; Kowalczyk, B.; Kandere-Grzybowska, K.; Borkowska, M.; Grzybowski, B. A. Engineering Gram Selectivity of Mixed-Charge Gold Nanoparticles by Tuning the Balance of Surface Charges. *Angew. Chem., Int. Ed.* **2016**, *128*, 8752−8756.

(26) Beaussart, A.; Beloin, C.; Ghigo, J.-M.; Chapot-Chartier, M.-P.; Kulakauskas, S.; Duval, J. F. L. Probing The Influence of Cell Surface Polysaccharides on Nanodendrimer Binding to Gram-Negative and Gram-Positive Bacteria Using Single-Nanoparticle Force Spectroscopy. *Nanoscale* **2018**, *10*, 12743−12753.

(27) Lyden, A.; Lombardi, L.; Sire, W.; Li, P.; Simpson, J. C.; Butler, G.; Lee, G. U. Characterization of Carboxylate Nanoparticle Adhesion with the Fungal Pathogen *Candida albicans*. *Nanoscale* **2017**, *9*, 15911−15922.

(28) Kontturi, E.; Laaksonen, P.; Linder, M. B.; Nonappa; Gröschel, A. H.; Rojas, O. J.; Ikkala, O. Advanced materials through assembly of nanocelluloses. *Adv. Mater.* **2018**, *30*, 1703779.

(29) Missoum, K.; Belgacem, M.; Bras, J. Nanofibrillated cellulose surface modification: A Review. *Materials* **2013**, *6*, 1745−1766.

(30) Zhang, Y.; Nypelö, T.; Salas, C.; Arboleda, J.; Hoeger, I. C.; Rojas, O. J. Cellulose nanofibrils: From strong materials to bioactive surfaces. *J. Renewable Mater.* **2013**, *1*, 195−211.

(31) Lin, N.; Dufresne, A. Nanocellulose in biomedicine: Current status and future prospect. *Eur. Polym. J.* **2014**, *59*, 302−325.

(32) Chen, W.; Yu, H.; Lee, S.-Y.; Wei, T.; Li, J.; Fan, Z. Nanocellulose: a promising nanomaterial for advanced electrochemical energy storage. *Chem. Soc. Rev.* **2018**, *47*, 2837−2872.

(33) Österberg, M.; Vartiainen, J.; Lucenius, J.; Hippi, U.; Seppälä, J.; Serimaa, R.; Laine, J. A Fast method to produce strong NFC films as a platform for barrier and functional materials. *ACS Appl. Mater. Interfaces* **2013**, *5*, 4640−4647.

(34) Ning, R.; Wu, C.-N.; Takeuchi, M.; Saito, T.; Isogai, A. Preparation and characterization of zinc oxide/TEMPO-oxidized cellulose nanofibril composite films. *Cellulose* **2017**, *24*, 4861−4870.

(35) Lizundia, E.; Goikuria, U.; Vilas, J. L.; Cristofaro, F.; Bruni, G.; Fortunati, E.; Armentano, I.; Visai, L.; Torre, L. Metal Nanoparticles Embedded in Cellulose Nanocrystal Based Films: Material Properties and Post-use Analysis. *Biomacromolecules* **2018**, *19*, 2618−2628.

(36) Díez, I.; Eronen, P.; Österberg, M.; Linder, M. B.; Ikkala, O.; Ras, R. H. A. Functionalization of nanofibrillated cellulose with silver nanoclusters: fluorescence and antibacterial activity. *Macromol. Biosci.* **2011**, *11*, 1185−1191.

(37) Missoum, K.; Sadocco, P.; Causio, J.; Belgacem, M. N.; Bras, J. Antibacterial activity and biodegradability assessment of chemically grafted nanofibrillated cellulose. *Mater. Sci. Eng., C* **2014**, *45*, 477−483.

(38) Saini, S.; Sillard, C.; Naceur Belgacem, M.; Bras, J. Nisin anchored cellulose nanofibers for long term antimicrobial active food packaging. *RSC Adv.* **2016**, *6*, 12422−12430.

(39) Saini, S.; Belgacem, M. N.; Bras, J. Effect of variable aminoalkyl chains on chemical grafting of cellulose nanofiber and their antimicrobial activity. *Mater. Sci. Eng., C* **2017**, *75*, 760−768.

(40) Jack, A. A.; Nordli, H. R.; Powell, L. C.; Farnell, D. J. J.; Pukstad, B.; Rye, P. D.; Thomas, D. W.; Chinga-Carrasco, G.; Hill, K. E. Cellulose Nanofibril Formulations Incorporating a Low-Molecular-Weight Alginate Oligosaccharide Modify Bacterial Biofilm Development. *Biomacromolecules* **2019**, *20*, 2953−2961.

(41) Koivuniemi, R.; Hakkarainen, T.; Kiiskinen, J.; Kosonen, M.; Vuola, J.; Valtonen, J.; Luukko, K.; Kavola, H.; Yliperttula, M. Clinical Study of Nanofibrillar Cellulose Hydrogel Dressing for Skin Graft Donor Site Treatment. *Adv. Wound Care* **2020**, *9*, 199−210.

(42) Fallarero, A.; Skogman, M.; Kujala, J.; Rajaratnam, M.; Moreira, V.; Yli-Kauhaluoma, J.; Vuorela, P. (+)-Dehydroabietic acid, an abietane-type diterpene, inhibits *Staphylococcus aureus* biofilms *in vitro*. *Int. J. Mol. Sci.* **2013**, *14*, 12054−12072.

(43) Helfenstein, A.; Vahermo, M.; Nawrot, D. A.; Demirci, F.; İşcan, G.; Krogerus, S.; Yli-Kauhaluoma, J.; Moreira, V. M.; Tammela, P. Antibacterial profiling of abietane-type diterpenoids. *Bioorg. Med. Chem.* **2017**, *25*, 132−137.

(44) Vahermo, M.; Krogerus, S.; Nasereddin, A.; Kaiser, M.; Brun, R.; Jaffe, C. L.; Yli-Kauhaluoma, J.; Moreira, V. M. Antiprotozoal activity of dehydroabietic acid derivatives against *Leishmania donovani* and *Trypanosoma cruzi*. *MedChemComm* **2016**, *7*, 457−463.

(45) Manner, S.; Vahermo, M.; Skogman, M. E.; Krogerus, S.; Vuorela, P. M.; Yli-Kauhaluoma, J.; Fallarero, A.; Moreira, V. M. New derivatives of dehydroabietic acid target planktonic and biofilm bacteria in *Staphylococcus aureus* and effectively disrupt bacterial membrane integrity. *Eur. J. Med. Chem.* **2015**, *102*, 68−79.

(46) Belu, A. M.; Graham, D. J.; Castner, D. G. Time-of-Flight Secondary Ion Mass Spectrometry: Techniques and Applications for the Characterization of Biomaterial Surfaces. *Biomaterials* **2003**, *24*, 3635−3653.

(47) Kempson, I. M.; Prestidge, C. A. Mass Spectrometry Imaging of Pharmaceuticals: From Tablets to Tissues. In *Analytical Techniques in the Pharmaceutical Sciences*; Müllertz, A., Perrie, Y., Rades, T., Eds. Springer New York: New York, NY, 2016; pp 629−647.

(48) Zimmermann, R.; Dukhin, S. S.; Werner, C.; Duval, J. F. L. On the use of electrokinetics for unraveling charging and structure of soft planar polymer films. *Curr. Opin. Colloid Interface Sci.* **2013**, *18*, 83−92.

(49) Zimmermann, R.; Kuckling, D.; Kaufmann, M.; Werner, C.; Duval, J. F. L. Electrokinetics of a Poly(*N*-isopropylacrylamid-*co*-carboxyacrylamid) Soft Thin Film: Evidence of Diffuse Segment Distribution in the Swollen State. *Langmuir* **2010**, *26*, 18169−18181.

(50) Law, K.-Y. Definitions for Hydrophilicity, Hydrophobicity, and Superhydrophobicity: Getting the Basics Right. *J. Phys. Chem. Lett.* **2014**, *5*, 686−688.

(51) Van den Driessche, F.; Brackman, G.; Swimberghe, R.; Rigole, P.; Coenye, T. Screening a repurposing library for potentiators of antibiotics against *Staphylococcus aureus* biofilms. *Int. J. Antimicrob. Agents* **2017**, *49*, 315−320.

(52) Dogsa, I.; Tomšič, M.; Orehek, J.; Benigar, E.; Jamnik, A.; Stopar, D. Amorphous supramolecular structure of carboxymethyl cellulose in aqueous solution at different pH values as determined by rheology, small angle X-ray and light scattering. *Carbohydr. Polym.* **2014**, *111*, 492−504.

(53) Wimley, W. C. Describing the mechanism of antimicrobial peptide action with the interfacial activity model. *ACS Chem. Biol.* **2010**, *5*, 905−917.

(54) Otzen, D. E. Biosurfactants and surfactants interacting with membranes and proteins: Same but different? *Biochim. Biophys. Acta* **2017**, *1859*, 639−649.

(55) Schlag, M.; Biswas, R.; Krismer, B.; Kohler, T.; Zoll, S.; Yu, W.; Schwarz, H.; Peschel, A.; Götz, F. Role of staphylococcal wall teichoic acid in targeting the major autolysin Atl. *Mol. Microbiol.* **2010**, *75*, 864−873.

(56) Ledala, N.; Wilkinson, B.; Jayaswal, R. Effects of oxacillin and tetracycline on autolysis, autolysin processing and atl transcription in *Staphylococcus aureus*. *Int. J. Antimicrob. Agents* **2006**, *27*, 518−524.

(57) Borišek, J.; Pintar, S.; Ogrizek, M.; Grdadolnik, S. G.; Hodnik, V.; Turk, D.; Perdih, A.; Novič, M. Discovery of (phenylureido)-piperidinyl benzamides as prospective inhibitors of bacterial autolysin E from *Staphylococcus aureus*. *J. Enzyme Inhib. Med. Chem.* **2018**, *33*, 1239−1247.

(58) Hassan, G.; Forsman, N.; Wan, X.; Keurulainen, L.; Bimbo, L. M.; Johansson, L.-S.; Sipari, N.; Yli-Kauhaluoma, J.; Zimmermann, R.; Stehl, S.; Werner, C.; Saris, P. E. J.; Österberg, M.; Moreira, V. M. Dehydroabietylamine-based Cellulose Nanofibril Films: A new Class of Sustainable Biomaterials for Highly Efficient, Broad-Spectrum Antimicrobial Effects. *ACS Sustainable Chem. Eng.* **2019**, *7*, 5002−5009.

(59) Kolsi, L. E.; Krogerus, S.; Brito, V.; Rüffer, T.; Lang, H.; Yli-Kauhaluoma, J.; Silvestre, S. M.; Moreira, V. M. Regioselective Benzylic Oxidation of Aromatic Abietanes: Application to the Semisynthesis of the Naturally Occurring Picealactones A, B and C. *ChemistrySelect* **2017**, *2*, 7008−7012.

(60) Johansson, L.-S.; Campbell, J. M. Reproducible XPS on biopolymers: cellulose studies. *Surf. Interface Anal.* **2004**, *36*, 1018−1022.

(61) Fischer, E. R.; Hansen, B. T.; Nair, V.; Hoyt, F. H.; Dorward, D. W. Scanning electron microscopy. *Curr. Protoc. Microbiol.* **2012**, *25*, 2B.2.1−2B.2.47.

(62) Brackman, G.; Garcia-Fernandez, M. J.; Lenoir, J.; De Meyer, L.; Remon, J.-P.; De Beer, T.; Concheiro, A.; Alvarez-Lorenzo, C.; Coenye, T. Dressings Loaded with Cyclodextrin-Hamamelitannin Complexes Increase *Staphylococcus aureus* Susceptibility Toward Antibiotics Both in Single as well as in Mixed Biofilm Communities. *Macromol. Biosci.* **2016**, *16*, 859−869.

(63) European Committee for Antimicrobial Susceptibility Testing (EUCAST) of the European Society of Clinical Microbiology and Infectious Diseases (ESCMID). Determination of minimum inhibitory concentrations (MICs) of antibacterial agents by broth dilution. *Clin. Microbiol. Infect.* **2003**, *9*, ix−xv.